
3D SCENE GEOMETRY ESTIMATION FROM 360° IMAGERY: A SURVEY

Thiago L. T. da Silveira, Paulo G. L. Pinto, Jeffri E. M. Llerena, Cláudio R. Jung
Institute of Informatics, Federal University of Rio Grande do Sul, Brazil
{tltsilveira, paulo.pinto, jeffri.mllerena, crjung}@inf.ufrgs.br

ABSTRACT

This paper provides a comprehensive survey on pioneer and state-of-the-art 3D scene geometry estimation methodologies based on single, two, or multiple images captured under the omnidirectional optics. We first revisit the basic concepts of the spherical camera model, and review the most common acquisition technologies and representation formats suitable for omnidirectional (also called 360°, spherical or panoramic) images and videos. We then survey monocular layout and depth inference approaches, highlighting the recent advances in learning-based solutions suited for spherical data. The classical stereo matching is then revised on the spherical domain, where methodologies for detecting and describing sparse and dense features become crucial. The stereo matching concepts are then extrapolated for multiple view camera setups, categorizing them among light fields, multi-view stereo, and structure from motion (or visual simultaneous localization and mapping). We also compile and discuss commonly adopted datasets and figures of merit indicated for each purpose and list recent results for completeness. We conclude this paper by pointing out current and future trends.

Keywords Omnidirectional Images · 360° Images · 3D Scene Geometry Estimation · Deep Learning · Depth Estimation · Layout Estimation

1 Introduction

The world is three-dimensional (3D). As such, recovering 3D information about real-world objects allows the exploration of many relevant applications, including self-driving cars [1, 2], robot navigation [3, 4], virtual tourism [5, 6], infrastructure inspection [7, 8], archaeological [9, 10] and architectural modeling [5, 11], city planning [12, 13], and 3D cinema [14, 15].

Many sensors can be used to obtain 3D data from real objects, such as light detection and ranging [16], structured light [17], and time of flight [18]. There is a plethora of approaches for inferring 3D information from plain color images/videos. The widespread accessibility and low-cost of consumer cameras is a strong motivation for the continued research efforts devoted to image-based 3D scene reconstruction methods [19]. In theory, 3D information can only be inferred from two or more captures of the scene, as in typical multi-view stereo [20] or structure from motion [21] approaches. However, recent approaches are exploring machine learning to perform *single-image* depth inference [22, 23, 24]. Most methods developed so far rely on traditional perspective/pinhole-based cameras, which have a narrow field of view (FoV) and thus might require thousands of captures to model large scenes [25, 26].

Unlike pinhole cameras, *truly omnidirectional* cameras capture the light intensities from the entire surrounding environment ($360^\circ \times 180^\circ$) at once [27, 28]. Thus, from the application point of view, only two captures might be necessary for recovering 3D information from the whole scenario (except for occlusions and disocclusions) based on triangulation-like algorithms [29] or even a single capture might be needed when using modern deep learning approaches [30]. Although catadioptric sensors date from the early 1970s [31], the recent release of affordable devices for capturing and visualizing *full FoV* media besides the novel augmented, mixed and virtual (AR/MR/VR) applications are inciting both the scientific community and the industry to invest efforts in novel technological solutions. Popular

consumer-grade cameras include the Samsung Gear 360¹ and the Ricoh Theta², whereas examples of head-mounted displays are the Samsung Gear VR³ and the Oculus Rift⁴. It is worth mentioning that the existing nomenclature for 360 images is vast, and the terms omnidirectional [32, 33], spherical [34, 35], full panorama [36, 27], and 360° [37, 28] images/videos/cameras are often used as synonyms.

360° images are intrinsically defined on the sphere surface and present three-degrees of freedom (3-DoF) natively, associated with the rotation angles pitch, yaw, and roll. This allows, for instance, head-mounted displays users to look at any direction of the captured view by performing rotational head movements. However, restricting the movements only to rotations may break the immersion sense when the observer’s head translates and the rendered scene mismatches, causing discomfort and sickness [15]. Although most head-mounted displays support 6-DoF tracking [28], the vast majority of real capture content is monoscopic [27], so that full immersion is mostly experienced on computer-generated imagery [38]. Depth perception is accomplished by presenting a stereoscopic image pair restricted to the user eye’s viewport, which may reduce the discomfort [39]. For allowing *small* head translational movements, both color (often called texture) and depth (or disparity) information must be provided for that specific virtual camera (and user) location. This still limited application scenario is called 3-DoF+ [40, 41], but approximates the full 6-DoF-enabled navigation, where colored 3D information is required for every possible location within the scene [42].

Estimating 3D scene geometry from 360° imagery allows to address all the classical problems mentioned in the first paragraph of this paper and is also pivotal for providing full immersive experiences to head-mounted displays users in novel AR/MR/VR-based applications. Despite the benefits of presenting full FoV, both the capture sensors (CCD, CMOS) and the representation formats (equirectangular images or cube-maps) for spherical images involve a regular rectangular 2D grid. As such, omnidirectional media present heavy non-affine distortions that are inherent to the spherical camera model [43]. Therefore, most of the image processing and computer vision algorithms developed in the past – which were designed to work with perspective images – tend to fail when directly applied to omnidirectional media, regardless of their objective [44, 45, 30, 14]. In this context, there is a growing number of works trying to bridge this gap by employing geometry- and learning-based approaches for recovering 3D information from one, two, or more full panoramas. How these applications are explored in immersive media is discussed throughout the text and summarized in the conclusions (Section 7).

This survey paper aims to briefly review the spherical imaging model (along with common acquisition pipelines and representation formats), and then focus on a comprehensive analysis of representative methods that tackle the 3D geometry estimation problem using one or more 360° images. A secondary goal is to compile meaningful publicly available datasets up to date, as well as the most widely accepted evaluation metrics for comparing the existing techniques.

1.1 Comparison with Existing Surveys

The survey by Gledhill and colleagues [46] revises pinhole-based approaches applied to image sequences taken by rotating cameras for composing *incomplete* panoramic images via stitching. The authors only acknowledge the existence of pairs of opposite-located fisheye lenses and complex catadioptric systems. The revised 3D reconstruction techniques are limited to approaches for triangulation of features matched in two or more perspective images, *i.e.*, traditional (multi-view) stereo matching, and the use of panoramas is mentioned as a trending topic.

Payá *et al.* [47] survey techniques for visual localization and mapping problems in the particular context of mobile robotics. They refer to “omnidirectional” imagery, but the reviewed works rely on catadioptric systems that do not cover the full vertical FoV and often represent the captured information by cylindrical projection. Furthermore, most of the revisited methods rely on a preprocessing step for “undistort” the images captured by the catadioptric systems since they cannot handle deformations.

Pintore and colleagues [48] review recent approaches for automatic 3D reconstruction of structured indoor scenarios focusing on the diversity of input modalities (color, depth or multimodal). They mention the advantages of working with full-FoV panoramas and the benefits of achieving registered depth information, highlighting the growing number of data-driven methods that tackle color images only and pointing out a very special niche of learning-based approaches that can infer the 3D scene layout from indoor panoramas. Similarly, the survey paper from Zou and colleagues [49] also concentrates on describing 3D layout recovery approaches. Related works addressed in [48, 49] are also revisited in our survey paper.

¹<https://www.samsung.com/global/galaxy/gear-360/>

²<https://theta360.com/en/>

³<https://www.samsung.com/global/galaxy/gear-vr/>

⁴<https://www.oculus.com/rift/>

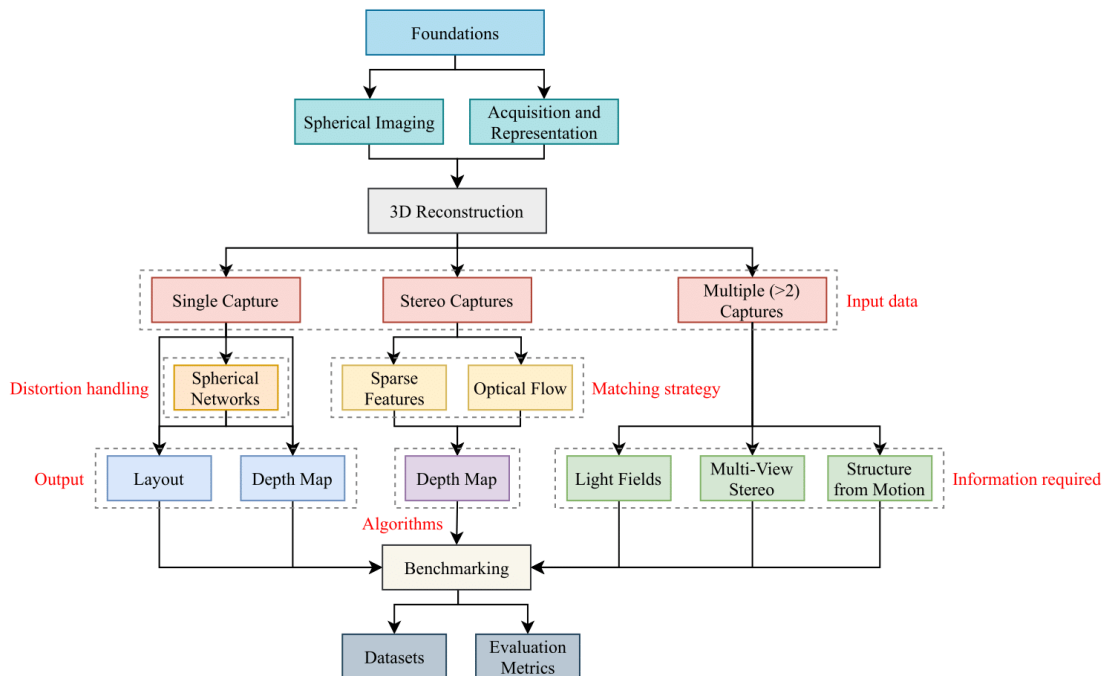


Figure 1: Paper Organization Diagram

Kang *et al.* [50] review recent approaches that use either pinhole-based cameras or active sensing for 3D reconstruction of indoor environments. The authors compile the most commonly used datasets for assessing methods dealing with one, two, or multiple views. The authors divide their analysis into approaches based on geometric and topological aspects or semantics for estimating the 3D scene geometry. However, only a few methods for depth or layout estimation based on panoramic images are revisited in their work, disregarding the particularities of the spherical camera model. In fact, the authors do not explicitly recognize as a trend the use of the emerging 360° image-based approaches for reconstructing the 3D geometry of scenes.

To the best of our knowledge, the current survey paper is the first to compile a comprehensive review of state-of-the-art approaches for 3D scene geometry recovery relying on one, two or multiple panoramas, focusing on either indoor or outdoor scenarios. This paper does not intend to review methods suited for perspective imagery. For that aim, the reader is redirected to relevant survey papers such as [51, 52] for monocular depth inference, [22, 23, 24] for stereo matching, [53] for light fields-based depth estimation, [20, 54] for multi-view stereo, and [21, 55, 56] for structure from motion or visual simultaneous localization and mapping.

1.2 Organization of this Paper

The rest of this survey paper is organized as follows. Section 2 firstly revisits the basic concepts of spherical imaging, the common acquisition pipelines, and the image representation formats often employed in the literature. Sections 3, 4, and 5 discuss techniques for recovering 3D geometry from scenarios and are organized according to the complexity of the traditional image capturing setup. More precisely, approaches for 3D geometry prediction from a single 360° image are examined throughout Section 3. More precisely, Section 3.2 discusses the methods targeting 3D layout inference, whereas Section 3.3 reviews techniques aiming for pixel-wise depth estimates. Since most methods that deal with a single panorama rely on neural networks, we also present in Section 3.1 a discussion on how to adapt planar networks to the spherical domain. Methods that rely on pairs of spherical images for 3D scene reconstruction are reviewed along Section 4. Since most of these approach require sparse or dense correspondences, we also revisit existing approaches for sparse keypoint detection and matching and optical flow estimation, both considering the spherical domain, in Sections 4.1 and 4.2, respectively. Section 5 focuses on techniques designed for recovering 3D information from multiple omnidirectional captures of the environment. Multi-view-based approaches are grouped according to the primary camera setups: light fields, multi-view stereo, and structure from motion, and are separately addressed in Sections 5.1, 5.2 and 5.3, respectively. Section 6 compiles a list of publicly available datasets, commonly used assessment metrics and protocols for different scenarios and 3D representations as well as selected state-of-the-art results. Finally, Section 7 concludes this survey paper, pointing out some of the recent trends towards 360° media

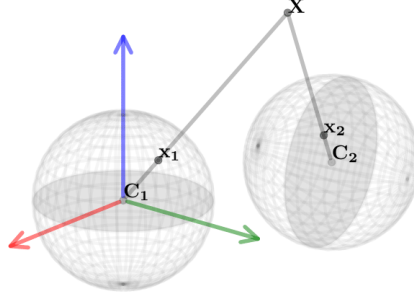


Figure 2: Projection of a world point onto two spherical cameras with different extrinsic parameters.

depth-awareness and its integration to fully immersive VR/AR/MR experiences. Fig. 1 provides a schematic illustration about the content organization adopted in this survey article.

2 Foundations, Acquisition and Representation of Spherical Images

This section revisits the basic concepts of the spherical camera model, the commonly involved acquisition tools and devices, and the most meaningful representation formats for spherical media. All the information gathered throughout this section paves the way for further discussing the single-view-, stereo-, and multi-view-based approaches that estimate 3D geometry from panoramas.

2.1 Spherical imaging

Capturing the light intensities from the whole (full-FoV) surrounding 3D environment (world) is accomplished by spherical projection [57], which leads us to the concept of spherical imaging [58, 59]. A spherical camera is modeled as an *unit sphere*, having no intrinsic parameters, and, thus, being fully represented by its extrinsics [60, 61].

For the mathematical characterization of the spherical imaging, let us consider a world point $\mathbf{X} \in \mathbb{R}^3$ and a spherical camera centered at $\mathbf{C} \in \mathbb{R}^3$, both positions w.r.t. a preset world coordinate system. The camera extrinsics $[\mathbf{R}|\mathbf{t}]$ are explained as $\mathbf{R} \in SO(3)$ being a rotation matrix and $\mathbf{t} = -\mathbf{R}\mathbf{C} \in \mathbb{R}^3$ being a translation vector relative to that world coordinate system. The projection of a world point \mathbf{X} onto a spherical camera parameterized by $[\mathbf{R}|\mathbf{t}]$ results on a point $\mathbf{x} \in S^2 \subset \mathbb{R}^3$ [62]:

$$\mathbf{x} = \frac{\mathbf{R}\mathbf{X} + \mathbf{t}}{\|\mathbf{R}\mathbf{X} + \mathbf{t}\|_2}. \quad (1)$$

Fig. 2 illustrates a world point \mathbf{X} projected onto two spherical cameras. One of them is centered at the origin of and aligned to the world coordinate system, *i.e.*, its extrinsic parameters are $[\mathbf{R}_1 = \mathbf{I}|\mathbf{t}_1 = -\mathbf{R}_1\mathbf{C}_1 = \mathbf{0}]$. The other is not at the origin and might be rotated, presenting extrinsic parameters given by $[\mathbf{R}_2|\mathbf{t}_2 = -\mathbf{R}_2\mathbf{C}_2 \neq \mathbf{0}]$. The projections \mathbf{x}_1 and \mathbf{x}_2 represent local image coordinates (*w.r.t.* each camera), and do not contain explicit information about the camera poses *w.r.t.* the preset world coordinate system.

From a geometric point of view, recovering the relative motion between two cameras can be explored by the coplanarity property, which associates correspondent image points and cameras centers [62]. The epipolar geometry describes the *geometrical* relation between a pair of central projection cameras capturing a static scene [63]. Since an omnidirectional camera is a central projection camera, so as pinhole-based ones are, this definition also applies to the spherical camera model [10]. Knowing the relative camera pose for two captures allows recovering the actual 3D points by geometrical reasoning.

Let us consider \mathbf{x}_1 and \mathbf{x}_2 as projections of \mathbf{X} onto two spherical cameras, as depicted in Fig. 2. We can consider that the first camera is *canonical*, *i.e.*, it is located at the origin of the world coordinate system and aligned to it. Since spherical cameras have no intrinsic parameters – *i.e.*, the Essential \mathbf{E} and the Fundamental matrices \mathbf{F} are the same – the projections \mathbf{x}_1 and \mathbf{x}_2 are related according to [57, 9, 62, 64]

$$\mathbf{x}_2^\top \mathbf{E} \mathbf{x}_1 = 0, \quad \mathbf{E} = [\mathbf{t}]_\times \mathbf{R}, \quad (2)$$

where $[\mathbf{t}]_\times$ is the skew-symmetric matrix corresponding to the cross-product with \mathbf{t} [60, 34]. Since \mathbf{E} is defined up to an unknown scale [65], only five from the six DoFs involving both the cameras can be resolved by exploring the epipolar constraint.

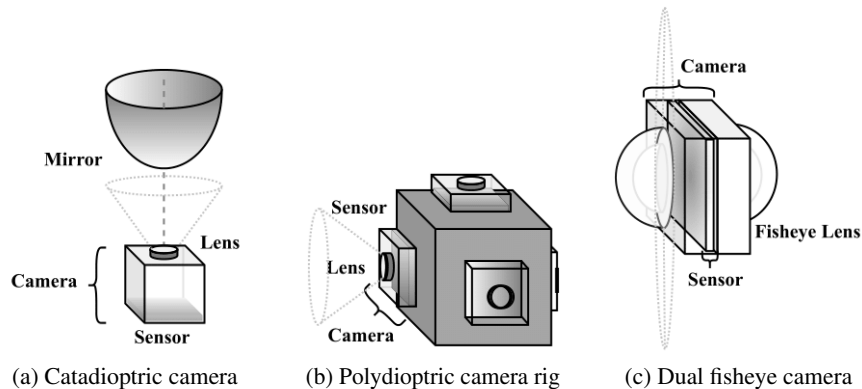


Figure 3: Popular omnidirectional capture setups. Dotted cylindroids represent the FoV of each lens.

There are many strategies for estimating \mathbf{E} from pairs of correspondences [66, 67, 65]. Several approaches [9, 7, 41] use the traditional eight-point algorithm (8-PA) [68, 66] to infer the Essential matrix, and some of them refine the estimates using non-linear optimization [60, 28, 9]. Obtaining the relative poses $[\mathbf{R}|\mathbf{t}]$ and the underlying 3D world points \mathbf{X}^k from a set of k *noiseless* correspondence points \mathbf{x}_1^k and \mathbf{x}_2^k and the recovered Essential matrix \mathbf{E} is straightforward [69, 63]. It is worth mentioning that dense correspondences on the sphere are hardly ambiguous in terms of epipolar geometry [70] and that even the 8-PA might produce accurate estimates for the Essential matrix if the correspondence points well distributed on the sphere [34].

As the reader will see in Section 3, many works try to estimate the distance connecting the camera center to the actual 3D point (*i.e.*, its depth) from single color panorama, mostly relying on paired color plus depth datasets to train a deep-learning model. Unlike approaches based on geometric aspects relating two or more cameras, learning-based methods might not rely on keypoint correspondences and triangulation. Different approaches for single-view 3D scene geometry recovery explore particular aspects of the spherical projection, and are further discussed in Section 3.

2.2 Acquisition and Representation

Although the spherical camera model provides a mathematical formulation for omnidirectional vision, there is no such *single-sensor device* for capturing all the scene information at once. The signals are still captured on a planar silicon surface that might result in a heavily distorted output image [71].

Catadioptric cameras, illustrated in Fig. 3(a), associate a perspective camera with convex-shaped (conic, spherical, parabolic, or hyperbolic) mirrors [19, 27], and introduced the idea of capturing the full horizontal FoV [72]. However, due to its sensor/mirror self-occlusions, these cameras are incapable of capturing the full vertical FoV [73], and the images are commonly represented through cylindrical projections [16, 44]. A compromise solution for increasing the represented FoV relies on catadioptric camera rigs [74]. It is possible to warp the scene captures and represent the (incomplete) image on the sphere if the intrinsic parameters of these cameras are known [62]. Although most classical approaches rely on bulky and costly equipment, recent works like [75] focus on portable mobile-aided solutions. Catadioptric cameras cannot capture the full-FoV, have fragile mirror components and are thus rare in recent scientific articles or industry applications.

A polydioptric imaging setup is a collection of an arbitrary number of regular cameras organized in a rig that might capture the whole surrounding scenario, as illustrated in Fig. 3(b). These camera rigs are often associated with a software-based solution for image stitching (mosaicking) that composes a panoramic image from the multiple captures [27, 32]. Compact camera rigs are often coupled to a rotating base for capturing stereoscopic panoramas with small vertical FoV or employ multiple fish-eye lenses for wider-FoV vision [76, 6, 3]. Professional devices can produce high-quality panoramic images but are expensive and demand a time-consuming post-processing step for image stitching [5]. Prominent examples include the Panono camera⁵, the Vuze camera⁶, the Facebook Surround360⁷, and the GoPro Odyssey⁸.

⁵<https://www.panono.com/>

⁶<https://vuze.camera/camera/vuze-camera>

⁷<https://github.com/facebook/Surround360>

⁸<https://gopro.com/en/us/news/here-is-odyssey>

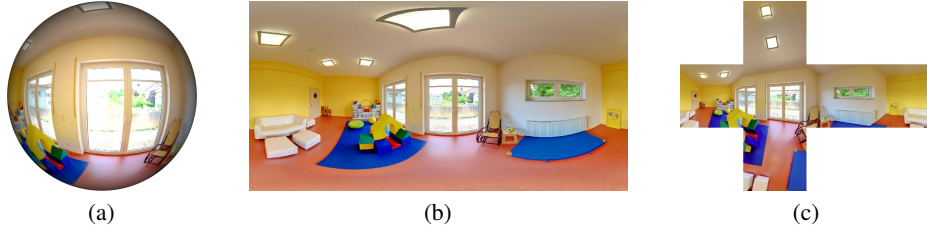


Figure 4: Ominidirectional image representations: (a) a spherical image (projected orthographically) and its mapping to (b) equirectangular and (c) cube-map formats. Sample image taken from the SUN360 dataset [84].

More recently, many manufacturers introduced cheap and portable devices equipped with two opposite located wide-FoV fish-eye lenses [27, 45, 77], and a schematic illustration is shown in Fig. 3(c). Each sensor captures a hemispherical image with a diagonal FoV slightly larger than 180°, producing overlapping regions that are suitable for two-image full-FoV stitching [78, 79]. These affordable cameras greatly democratized and simplified the acquisition of real-world 360° content [80]. The facilitated access to full-FoV imagery boosted the AR/VR/MR industry and research on related fields. Examples of those capturing devices are the Ricoh Theta, the Samsung Gear 360, the Insta360 cameras⁹, the LG 360 CAM¹⁰, and the Nikon Keymission 360¹¹.

In summary, catadioptric cameras have a historical value but are no longer widely considered for omnidirectional imaging. Polydioptric camera rigs are expensive and bulky, but can produce high-resolution panoramas. Dual-fisheye sensors are cheaper and more compact, but with limited resolution. Hence, the choice for a given capture device depends on the target application. In fact, most papers (particularly those that require single panoramas) do not mention the capture process itself, but instead focus on the *representation* of the spherical images, as discussed next.

Because of the wide diversity of technologies employed for acquiring omnidirectional content, most computational methods prefer to work with a canonical format representation of the sphere. The equirectangular projection is known as the standard mapping of the sphere to the plane [35, 81] and it is widely employed among both camera vendors and researchers [45], allowing easy pixel mapping from plane to sphere (and vice-versa). In the formulation presented in Section 2.1, every imaged point \mathbf{x} lies on the surface of a unit sphere. Therefore, \mathbf{x} can be rewritten in terms of spherical coordinates ($r = 1, \theta, \phi$) as [62]

$$\mathbf{x} = [\cos \theta \sin \phi \quad \sin \theta \sin \phi \quad \cos \phi]^\top, \quad (3)$$

where $\theta \in [0, 2\pi)$ and $\phi \in [0, \pi)$. Since there is information associated to every position (θ, ϕ) on the sphere – *i.e.*, the light intensities captured by the spherical camera – the whole image can be organized in a $[0, 2\pi) \times [0, \pi)$ planar representation. More precisely, the intensity value from the projected point \mathbf{x} is mapped to an integer pixel position (x, y) of a $w \times h$ equirectangular image where $x = \lfloor \frac{\theta w}{2\pi} \rfloor$ and $y = \lfloor \frac{\phi h}{\pi} \rfloor$. The equirectangular mapping is equivalent to the so-called latitude-longitude maps [82, 83, 16], differing only by translation factors on θ and ϕ .

The equirectangular projection distorts the objects differently depending on their location on the imaged scene [44], particularly near the poles of the sphere [85]. These deformations result from the non-uniform sampling of the sphere [86]. There are other ways to represent the sphere on the plane, but all of them introduce some distortion as well [45]. In fact, the distortions induced by spherical projection depend on the FoV amplitude [87, 88]. A common approach for representing images with smaller deformation is to project a 90° vertical and horizontal FoV to each face of a cube circumscribed around the sphere. This format is known as cube-map projection [89, 87] or sky-box [90]. Fig. 4 depicts the mapping of a spherical image to its equirectangular and cube-map representations.

Emerging representations are based on successive divisions of a 3D geometric form and aim to mitigate even more the distortions from the spherical model. The fine-grained mesh based on an icosahedron [57, 86, 82, 91] is by far the most popular, and it is also known as icosphere [92] or tangent planes projection [43]. Octahedron-based 360° images are also found in the literature [86, 93]. It is worth mentioning that many other sphere-to-plane representations can be imported from cartography [43], but the resulting images can be built from an equirectangular input image. However, one may note that exchanging formats may induce loss of information and artifacts [14], mostly because of the interpolation operations needed to cope with sub-pixel transformations [81].

⁹<https://www.insta360.com/>

¹⁰<https://www.lg.com/us/mobile-accessories/lg-LGR105AVRZTS-360-cam>

¹¹<https://www.nikonusa.com/en/nikon-products/product-archive/action-camera/keymission-360.html>

Table 1: 3D geometry estimation methods based on a single spherical image.

Reference	Category	Representation	Technology	Density
Shum <i>et al.</i> [101]	Layout	ERP	Interactive	Sparse
Yang and Zhang [102]	Layout	TPP	Semi-interactive	Sparse
Jia and Li [103]	Layout	TPP	Optimization	Sparse
Fukano <i>et al.</i> [104]	Layout	CMP	Optimization	Sparse
Pintore <i>et al.</i> [105]	Layout	ERP	Optimization	Sparse
Xu <i>et al.</i> [106]	Layout	TPP	Bayesian Optimization	Sparse
Fernandez-Labrador <i>et al.</i> [4]	Layout	ERP	CNN/SCNN	Sparse
Fernandez-Labrador <i>et al.</i> [107]	Layout	TPP	Geometry/CNN	Sparse
Fernandez-Labrador <i>et al.</i> [108]	Layout	ERP	Geometry/CNN	Sparse
Zou <i>et al.</i> [109]	Layout	ERP	Geometry/CNN	Sparse
Yang <i>et al.</i> [95]	Layout	ERP/E2P	CNN/BLSTM	Sparse
Sun <i>et al.</i> [110]	Layout	ERP	DNN	Sparse
Pintore <i>et al.</i> [111]	Layout	2× E2P	CNN/BLSTM	Dense
Zou <i>et al.</i> [49]	Layout	ERP/E2P	Several	Sparse
Zioulis <i>et al.</i> [112]	Layout	ERP	DNN	Sparse
Yang and Zhang [113]	Layout/Depth	ERP	Optimization	Dense
Yang <i>et al.</i> [114]	Layout/Depth	TPP	CNN	Dense
Sun <i>et al.</i> [115]	Layout/Depth	ERP	DNN/Attention	Dense
Jin <i>et al.</i> [116]	Layout/Depth	ERP	CNN/Attention	Dense
Wang <i>et al.</i> [117]	Layout	ERP	DNN/BLSTM	Sparse
Silveira <i>et al.</i> [87]	Depth	TPP	DNN	Semi-dense
Zioulis <i>et al.</i> [118]	Depth	ERP	DNN	Dense
de La Garanderie <i>et al.</i> [100]	Depth	ERP	SDNN	Dense
Eder <i>et al.</i> [35]	Depth	ERP	DNN	Dense
Tateno <i>et al.</i> [30]	Depth	ERP	DNN	Dense
Zioulis <i>et al.</i> [37]	Depth	ERP	SDNN	Dense
Wang <i>et al.</i> [119]	Depth	ERP/CMP	SDNN	Dense
Lee <i>et al.</i> [93]	Depth	<i>SpherePHD</i>	SDNN	Dense
Jiang <i>et al.</i> [120]	Depth	ERP/CMP	DNN	Dense

In the remainder of this paper, we will refer to the equirectangular projection (ERP), cube-map projection (CMP), tangent planes projection (TPP), cylindrical projection (CP), and hemispherical projection (HP) by their acronyms here introduced. Other format representations, such as the SpherePHD [94] and Equirectangular to Perspective (E2P) [95], will be further explained since they are tightly coupled to the layout or depth estimation methodologies where they are defined.

3 Monocular 3D Geometry Estimation

Inferring depth from two or more views of a scene is a well-studied problem. The literature on *single-image stereo* for pinhole cameras is more recent, and one of the first methods that attempted to *learn* depth from color images was based on Markov Random Fields [96]. However, a new era started with the seminal work of Eigen *et al.* [97], who explored deep architectures for depth inference. Early approaches for room layout (sparse global 3D information) extraction from pinhole images rely on geometrical cues like vanishing lines and points [98], but results started to improve significantly with the use of deep learning [99].

The complete FoV of spherical images allows the estimation of full depth images or layout from a single capture. Methods based on spherical images can either cast the problem as a set of planar projections or directly work on the spherical domain. For the latter set of methods, deep learning is the dominant strategy nowadays, and several modifications have been proposed to traditional architectures so they can perform better on panoramas. This section starts by reviewing general approaches that adapt/tailor neural networks to handle panoramas better. Then, it revises techniques for 3D layout extraction and dense depth estimation using a single panorama.

Table 1 summarizes the single-panorama approaches reviewed in this section, highlighting: the main goal (layout or depth); the spherical representation used as input (ERP, CMP, TPP, E2P or *SpherePHD*, as described in this section, or the previous one); the core technology explored by the method (where DNN denotes a planar *deep neural network* with convolutional and possibly fully-connected layers, and SDNN indicates if some network adaptation to the spherical domain was used); and density of the produced 3D representation (mostly sparse or dense). Except for the works [30] and [100], all the others listed in Table 1 assume an indoor scene capture as input.

3.1 Spherical Neural Networks

Convolutional Neural Networks (CNNs) have been widely used in problems such as image classification, object detection, segmentation, and single-image depth estimation [121, 122, 97]. However, applying “planar” CNNs directly to panoramas presents some challenges. There are three major issues when applying planar CNNs to ERP images. First, these techniques do not take into account the circularity property of the ERP images, which may lead to horizontal discontinuities [123, 37]. Second, standard CNNs neglect the non-uniform sampling of ERP images and apply convolutional kernels (same applicable to poolings, etc.) of fixed size all over the image [45, 81]. For spherical images, particularly those in the ERP format, a larger receptive field would be desirable near the poles since they are oversampled. Third, most standard CNNs are trained using planar images, that when applied to panoramas might lead to domain gap issues and produce unsatisfactory results [30, 45, 87]. Applying standard CNNs to CMP images is also not straightforward. Each cube face has a smaller field of view (90°) but still contain heavy “radial” distortions, unlike most perspective images. Furthermore, the cube faces need to be processed individually and then stitched together back to the sphere. Such approaches commonly lead to discrepancies in each face and may demand a postprocessing step [87, 118]. Although our discussion focused on ERP and CMP representations, these considerations are valid to any sphere-to-(multi)plane mapping since they either present non-uniform sampling distortions or require stitching to cover the whole sphere.

Other researchers focused on designing spherical CNNs (SCNNs) that can better handle the distortions in 360° images. Next, we describe some recent methods that try to mitigate the non-uniform sampling problem in panoramas in a generic deep-learning perspective. *Not all these methods have been effectively explored in the context of 3D estimation using panoramas, but they can be potentially used in the future.*

A simple solution to handle the horizontal field-of-view circularly of spherical images in ERP format is to adapt a convolutional layer by adding circular padding, as explored in [124, 125]. This idea (or an alternative by applying a larger circular pad to the input panorama) was explored to obtain optical flows in [41] and 3D layout from a single panorama in [110, 112].

Some authors design SCNNs by using 3D spherical coordinates. For example, Cohen *et al.* [126] propose spherical convolutions, with the spherical coordinates represented in a 3D manifold. To achieve rotation invariance, the convolutions are performed in the spectral domain, and pooling is easily extended. Esteves *et al.* [127] achieves rotational equivariance by defining convolutions in the spherical harmonic domain. Both approaches were tested in classification tasks. As noted in [128], rotation-invariance is not always desired, like in the toy problem of differing digits “9” and “6” in the context of object classification. Furthermore, these networks present a computational overhead due to special functions like the Spherical Fourier Transform.

Other approaches use an approximation or sampling of the sphere. Defferrard *et al.* [94] uses HealPix sampling to represent the sphere and define the convolution in spectral-domain, where pooling is naturally extended. Similarly, Lee *et al.* [129] uses a geodesic representation to map the sphere and a triangle base as a pixel point where a proper convolution and pooling are easily defined, naming it as *SpherePHD*. Both works report outperforming results than planar CNNs in classification, object detection, and segmentation tasks, and later explored for depth estimation in [93].

Jiang *et al.* [128] perform convolutions using Parametrized Differential Operators designed for unstructured grids based on differential operators of different orders, which is more accurate than using only the immediate neighborhood as claimed by the authors. Zhao *et al.* [130] suggest a Direct Neighbor convolution that performs the convolution with seven values (direct neighbors and the “center of kernel”), duplicating values if necessary. Although these previous approaches are faster than networks defined directly on the sphere, employing an approximation based on icosahedrons produces tight constraints on the number of vertices: $n = 5 \times 2^{2l+1} + 2$ vertices are generated for a given subdivision l .

Other strategies were not designed specifically for spherical image processing, but can be adapted to deal with the non-uniform sampling issue. First, Liu *et al.* [131] propose a coordinate convolution layer (*CoordNet*) that adds coordinate information to the standard convolution to learn the pattern between the feature map and the associated spatial location. This strategy was explored for computing the optical flow in panoramas [132] and also for layout estimation in [112]. On the other hand, deformable kernels [133] have been explored in spherical imaging, where the kernel support is adapted according to each spatial location of the ERP image. Many authors employ this strategy in tasks involving panoramas, such as classification [81], depth estimation [30], saliency detection [134], and layout estimation [4].

Graph neural networks can inherently handle non-uniformly sampled data, and hence can be explored for panoramas. Frossard *et al.* [135] claim that a proper weight design is crucial for graph convolution operators to obtain the same graph signal response at different distortion levels. Although graph networks are very flexible *w.r.t.* the nodes (pixels) geometric distribution, their computation time is typically higher due to operations (e.g., pooling and convolutions) that act over irregular sampled data.

3.2 Layout Estimation

The main goal of layout estimation techniques is to obtain a sparse 3D representation of an *indoor* scene. In general, the rooms are modeled as cuboids (which can be a reasonable model for simpler rooms) or with a more general hypothesis such as Manhattan worlds. Spherical cameras are particularly interesting for this application since a single capture can be used as input.

Shum *et al.* [101] present a pioneer work for layout estimation from panoramas. They propose an interactive system in which the user draws primitives (points, lines, planes) that allows the estimation of the camera pose. Then, a set of constraints (such as known points or segments) are used to obtain the 3D representation. Yang and Zhang [102] introduce a semi-supervised approach for layout recovery. In the automatic part, narrower FoV views are extracted from the panorama, from which geometrical cues such as orientation maps and geometric context are computed. Candidate box layouts are projected onto the perspective views, where geometric cues are used to find the best box candidate. Finally, the extracted box can be manually edited to allow more generic Manhattan layouts. Fukano and colleagues [104] follow a similar approach: they project the panorama to the cube, compute line primitives for each face and combine them back in the panorama. These primitives are separated into potential plane boundaries or not through a global labeling approach, and plane-related segments are used to find the cuboid. Clearly, the need for manual interaction is a drawback of [101, 102], and the restriction to cuboids is a limitation of [104].

One of the first works on automatic cuboid layout estimation was proposed by Yang and Zhang [136]. They assume a full horizontal view panorama with a central horizon, which is divided into four non-overlapping sub-images that are later undistorted based on TPP. They explore a parameterization method based on vanishing polylines to encode all four layouts into a single full-room layout, which is predicted via parameter candidate evaluation using a linear scoring function. For training the weights of the scoring function, they use a structured Support Vector Machine (SVM) on a non-panoramic indoor image dataset. *PanoContext* [137] recovers a cuboid room layout, the bounding volumes and the semantics of common furniture. The core idea is to generate hypotheses for the room layout and object bounding volumes using lower-level information (edges, segmentation, orientation, and context) and rank them using an SVM. Although *PanoContext* expands the analysis over [136] by adding object bounding volumes, it also assumes a simple primitive for the box layout. *Pano2CAD* [106] extends the idea of [137] by allowing Manhattan layout models, enhancing the 3D object detection, and also adding context priors to relate pieces of objects (furniture) to walls. As in *PanoContext* [137], *Pano2CAD* focuses on images of living rooms and bedrooms, and the computational cost is high.

Geometric primitives are also explored by Jia and Li [103], who adapt the Canny edge detector to the spherical domain for finding line segments, corners and vanishing points. They use heuristic rules based on a combination of these primitives for generating a score function that leads to the desired 3D layout when maximized. Yang and Zhang [113] also explore line primitives, combining them with spherical superpixels (based on [138]) for inferring layout and depth. They assume planar depth values within the superpixels and impose constraints based on neighborhood and context (ground or wall) using a constrained linear least-squares formulation. Their output is not precisely a room layout, but a dense depth map built with Manhattan world assumptions, in which pixels present semantic labels (walls, ceiling, floor). Clearly, the results of [103, 113] are strongly dependent on the computation of the primitives, which might fail in low contrast/texture regions. Pintore and colleagues [105] also explore geometrical primitives but relaxed the Manhattan world assumption. Their method starts by labeling the panorama as walls, floor, and roof using [139]. Then, they propose a projection function to map image edges onto the ground floor (assuming known camera height), and use a Hough transform-like voting scheme to obtain the room shape. On the one hand, this approach is more generic for not assuming Manhattan worlds. On the other, it implicitly assumes that the panorama is gravity-aligned, which might not be accurate in practical situations [140].

The availability of larger annotated datasets, starting with the *PanoContext* dataset in 2014 [137], leveraged the development of deep learning approaches for layout estimation. However, applying CNNs directly to the ERP is not ideal due to both the space-varying distortions introduced by this projection near the poles and the loss of spatial correlation between the left and right extremities of the panorama [126]. As such, some deep learning methods for layout estimation explore or propose some kind of data or network adaptation to better explore the geometry of spherical images, as discussed next.

To the best of our knowledge, the first deep learning approaches for layout estimation date from 2018 and combine geometrical cues with deep networks. Fernandez-Labrador *et al.* [107] first extract vanishing points to upright align the panorama, and split it into 60 overlapping narrow-FoV perspective images. Then, they apply a pre-trained CNN [99] to each projection, extracting local edge maps that are stitched back to the panorama. Finally, they perform edge pruning, corner extraction, and classification to generate a Manhattan layout, noting that normal maps extracted from the perspective projections using [141] are used for refining the layout. *LayoutNet* [109] also explores geometrical cues and deep networks for layout estimation using a single (perspective or ERP) image. The authors firstly gravity-align the panorama, and then feed it to a two-branched encoder-decoder CNN with the same architecture: the first branch

provides wall-wall, ceiling-wall, and wall-floor boundary maps, whereas the second one predicts a corner map and receives skip-connections from the former. The CNN output feeds a 3D layout regressor that outputs the cuboid layout. Finally, *LayoutNet* uses geometric reasoning for refining the layout respecting the Manhattan world assumption. *PanoRoom* [108] builds on top of [107], but working directly on the ERP image. An encoder-decoder CNN with skip connections based on ResNet-50 predicts both corner and edge probability maps on separate output channels of a single branch. Geometric reasoning based on vanishing lines (as in [107]) estimates a Manhattan-constrained layout, showing superior quantitative results when compared to [137, 107, 109].

Other works propose end-to-end deep learning approaches that do not require additional geometric reasoning. *DuLa-Net* [95] explores an encoder-decoder architecture with two-branches, each one attaining a different panorama representation: one branch is fed with an ERP image and outputs both a floor-ceiling probability map and a layout height estimation; the other receives a perspective ceiling-view, computed by an Equirectangular to Perspective (E2P) algorithm, and outputs a floor plan probability map. The final 3D layout is computed by first transforming the panorama branch output using E2P, and separating floor and ceiling probability maps, which are combined with the ceiling-branch output map to create a fused floor plan probability map. The fused map and the estimated height allow the creation of the final 3D layout. According to the authors, *DuLa-Net* outperforms both *PanoContext* and *LayoutNet*. *HorizonNet* [110] encodes a panoramic layout using three vectors with the same dimension as the image width (in ERP format), which implicitly handles the distortions of spherical images along the rows. For each column, their representation provides the vertical coordinates of ceiling-wall and floor-wall boundaries, and the probability of wall-wall boundaries. As [107], *HorizonNet* employs a ResNet-50 backbone and explores column-wise recurrent information using a bidirectional long short-term memory (BLSTM). Finally, Manhattan world constraints are added to the network output for generating a closed layout. The follow-up study *HoHoNet* [115] also explored the idea of encoding layout (and depth) information along a column-wise vector, but as a latent representation extracted with a feature pyramid as backbone and combined by an attention layer [142]. The latent vector is then unwrapped to the 2D spatial domain using the inverse discrete cosine transform, enabling either layout or depth estimation. For layout estimation, they used the same strategy as [110], reporting state-of-the-art results. *LED²-Net* [117] also builds on top of [110] in terms of the network architecture. However, they encode the room layout as a set of equiangular (in terms of longitude) spaced rays on the floorplan (and ceiling), which leads to a differentiable loss function. Based on this “horizon-depth” representation, the 3D layout is obtained by extrusion assuming a gravity-aligned camera with approximately known height (plus a post-processing step to impose Manhattan worlds, as in [110]). The authors show state-of-the-art results on different datasets and an interesting cross-dataset validation experiment.

Moving toward the relaxation of geometric constraints of the layout, Pintore *et al.* [111] assume Atlanta worlds in which the room presents a horizontal floor and ceiling, but the vertical walls are not necessarily orthogonal to each other (they may even be curved). Their core idea is to project the panorama into planes above and below the camera (ceiling and floor projections), similarly to the E2P step used in [95]. They proposed an encoder-decoder architecture that takes floor (or ceiling) projections and regresses a binary mask segmenting the floor (or ceiling). Their network also uses a ResNet-50 backbone, followed by a reshaping step and a BLSTM layer that captures long-range patterns of the layout. Finally, a series of convolutional layers followed by linear interpolation decode the sequential feature map to the output binary mask. The 2D layout is a polygon approximation of the ceiling segmentation mask, and the room height is chosen as to maximize the correlation between the ceiling and floor projections. Their results for cuboid-like layouts are comparable to [95, 110], but improve as the layout complexity increases. *Corners for Layout* [4] can handle even more generic layouts by predicting pixel-wise heatmaps for both corners and edges, with the only assumption of floor-ceiling parallelism. These maps are regressed by two end-to-end fully convolutional encoder-decoder architectures with the same structure, including as an option the use of spherical convolutions (similar to [30]) to account for the distortions of the ERP format. Their experimental results demonstrate that their SDNN is more robust to distortions induced by camera alignment, but standard convolutions are competitive if the input panoramas are gravity-aligned. *Single-Shot Cuboids* [112] also regresses corners, but without any additional information or post-processing, at the cost of restricting the geometry to a cuboid. This allows end-to-end training using a network without any spherical adaptation except of circular padding (but exploring recent advances such as anti-aliasing pooling [143]). Their method is considerably lighter (in terms of parameters) than competitive approaches such [110, 4], but such simplicity comes with the cost of a cuboid-shaped layouts only.

Providing a full comparative analysis of layout extraction methods is a challenging task. There is a coupling between how generic the method is in terms of layout geometry (cuboid, Manhattan, Atlanta, no restriction) and the characteristics of the images in the evaluated datasets, which also relates to the availability of publicly available datasets and standardized metrics and annotations (see Section 6 for a discussion). Recently, Zou and collaborators [49] provided an in-depth comparative analysis of [109, 95, 110], discussing how these methods can be divided into similar components implemented with different strategies and what are the effects of each design decision on the results. They also propose improved versions of *LayoutNet* and *DuLa-Net* (named *LayoutNet v2* and *DuLa-Net v2*). Their analysis indicated that



Figure 5: Examples of layout estimation results. Color image (personal dataset) and different layout representations are overlaid for better visualization using (a) *DuLa-Net* [95], (b) *HorizonNet* [110], (c) *Corners for Layout* [4], and (d) *HoHoNet* [115]. Layout markers are depicted as meant by the authors in their publicly available codes.

the quantitative results achieved by the methods (particularly *LayoutNet v2* and *HorizonNet*) may vary considerably depending on the test dataset.

Fig. 5 shows the layout estimates for an unseen scenario (image from our personal dataset) obtained by four state-of-the-art approaches [95, 110, 4, 115]. The input ERP image and the estimates are overlaid for better visualization, and each estimate is represented as meant by the authors of the original papers [95, 110, 4, 115]. Fig. 5(a) distinguishes horizontal (ceiling and floor) and vertical layout edges, whereas Figs. 5(b), (c), and (d) present unified edge maps. Fig. 5(b) and (d) still generate a 1D probability map for the existence of wall-wall boundaries (thin grayscale image on the top).

3.3 Depth Estimation

One of the first works tackling the single-image depth estimation problem under the spherical optics can be found in [87], where the authors propose to extract and process multiple overlapping narrow-FoV planar projections from the spherical image. More precisely, each planar image is individually fed to a (black box) depth estimation method trained with perspective images and then the resulting depth maps are back-projected to the sphere. The minimization of depth differences and alpha-blending provides the final output. Despite the interesting results shown in [87], the stitching artifacts arise when merging adjacent tangent planes. The work from Yang *et al.* [114] also represents spherical images as a collection of narrower-FoV planar images. The authors extract geometric and semantic cues from the images and combine them for ground plane detection and occlusions reasoning. Their method uses extracted lines and superpixels to impose planarity constraints on the global scene layout under the Manhattan world assumption. Then, the finer details associated with typical indoor objects are estimated via depth propagation. de La Garanderie *et al.* [100] present an approach for adapting DNNs developed on perspective imagery to work with panoramas, focusing on object detection and depth estimation. Their main idea is to consider existing datasets of perspective images as patches that are projected onto the sphere using style transfer. Also, they provide a simple adaptation of traditional CNNs to deal with panoramas by circularly padding the horizontal boundaries of ERP images (as other works for layout estimation revised in Section 3.2). The transformed images, however, do not cover the full panorama, and it might affect tasks that require a broader spatial context.

OmniDepth [118] is a fully convolutional encoder-decoder network that explicitly accounts for the distortions of ERP images using dilated convolutions for adapting the receptive fields depending on the latitude. *OmniDepth* is trained in a completely supervised manner with ground truth depth maps. Distortions were also explicitly taken into account by Tateno *et al.* [30], who introduce a deformable convolutional filtering approach applicable to dense prediction tasks. Their filtering approach allows to train a CNN using regular convolutions and perspective imagery, and then transfer the weights to another network with the same architecture capable of deforming the convolutions for addressing the distortions present in ERP images. The authors report improved results regarding traditional CNNs (applied to either ERP or CMP images), where the artifacts are prominent. The study from Eder and colleagues [35] introduces a plane-aware encoder-decoder network that jointly estimates depth and normal maps from indoor scenarios. Besides the color image, the authors also supply the network with a latitude-longitude geodesic map that, as they claim, accounts for the irregular sampling of the ERP images (recall the main idea behind *CoordNet* [131]). In fact, the authors provide an ablation study showing a performance gain in normal map prediction.

Zioulis and colleagues [37] present a self-supervised scheme that minimizes depth-based photometric error instead of depth itself, similarly to [144] for perspective images. Given a panorama and the corresponding depth map, they used a depth image-based rendering (DIBR) approach tailored to the spherical domain to produce new synthetic views, emulating translational (vertical or horizontal) camera movement. To deal with distortions in the ERP format, they explored a backbone based on *CoordNet* [131], in which pixel coordinates are also used as input to the network.

Although the reported experimental validation is limited, the authors claim that their approach can better generalize to a wider range of images.

Some authors explore branching strategies for depth estimation. Wang *et al.* [119] takes advantage of both full-FoV ERP images and the less distorted CMP representation by using a two-branch encoder-decoder network (*BiFuse*), each one processing a different image representation (a spherical padding scheme was introduced to ensure continuity between adjacent faces of the CMP image in the second branch). They use *bi-projection fusion blocks* that allow a bi-directional flow of information between the two branches that yields better results according to the authors. *UniFuse* [120] builds on top of *BiFuse*, presenting two encoders, fed with ERP and CMP representations, and just one decoder. Unlike *BiFuse*, however, *UniFuse* unidirectionally feeds the CMP features to the ERP features at the beginning of the decoder, arguing that “optimizing the CMP depth may cause the training to lose focus on the ERP depth”. Jin *et al.* [116] explore a different branching strategy for jointly estimating the layout and the depth map of indoor scenes. Their network, which has planar convolutions, presents two stages: one that uses layout as a prior for estimating the depth, and another one that regularizes the depth map using the layout, assuming planar walls. A semantic segmentation scheme that predicts a furniture map is also used as an attention module to alleviate the influence of furniture in the regularization stage. Both [119] and [116] present better results when compared to *OmniDepth* [118]. Since they were published at the same conference, they do not compare with each other. However, the reported results in both methods for the Stanford 2D-3D-S dataset [145] are very similar, whereas *UniFuse* shows slightly better results.

It is also worth mentioning the non-Euclidean spherical polyhedron representation (*SpherePHD*) for panoramas presented in [129], and its extended version that tackled the depth inference problem in [93]. The *SpherePHD* structure represents a 360° image by triangular tessellation, in which each triangle individually has a small distortion. These triangles are then re-indexed and arranged so that conventional CNNs can be applied to the proposed representation. For depth estimation, the authors proposed an encoder-decoder scheme with residual layers using the new representation. Although they do show improved results *w.r.t.* ERP or CMP representations for this task, no comparison with other state-of-the-art approaches were provided (in fact, depth estimation was not the main goal of the paper, but used as a potential application).

Fig. 6 shows depth maps produced by three state-of-the-art monocular depth estimation methods [118, 119, 115] applied to panoramas captured in different scenarios. The selected images illustrate common and “unusual” indoor environments, as well as natural and urban outdoor scenes. Both real and synthetic captures are considered. The color image in the first row is a synthetic re-rendering of a 3D model based on real captures, available in the test split of the 3D60 [118] dataset. The color images in rows two to six are real captures taken from the SUN360 dataset [84], and the last color image is a capture from a synthetic model, available at the Urban Canyon [88] dataset. It is interesting to note that the depth maps produced by the approaches are consistent in the common indoor scenarios (first and second rows), but perform poorly in the other scene contexts. This behavior is highly related to the training datasets used in [118, 119, 115], which consist mainly of indoor panoramas with common decoration objects and furniture. Outdoor scenarios are less controlled, since the range of depth values is potentially larger, and may present pixels with an “infinite” depth (often misrepresented in ground truth depth maps of synthetic outdoor scenarios). As a result, only few works consider tackling this problem [30, 100] – which may obligate changing the methodology design and parametrization.

It is also important to mention that depth maps produced by single-panorama approaches present scale ambiguity. This problem is implicitly taken into account when all scenes present approximately the same dimensions (as in panoramas taken inside the rooms of a house, for example), but can also be explicitly handled if additional information is provided (*e.g.*, the height of the camera as in [105, 117]). In terms of quantitative evaluation, some metrics handle the scale ambiguity problem by performing some kind of depth adjustment in the comparison, as discussed in Section 6.2.2.

4 Stereoscopic 3D Geometry Estimation

Obtaining 3D information from a pair of images is inherent to human beings, who interpret disparities seen by both eyes as depth. The literature on stereo matching for perspective images is extensive, but the amount of papers that explore stereo panorama pairs is much smaller. On the one hand, there is a strong information overlap between the information captured by the two panoramas, unlike the scenario with narrow-FoV cameras. On the other hand, finding correspondences between two panoramas is harder due to the non-affine distortions introduced by the spherical projection. This section starts revising sparse and dense feature matching methods tailored to the spherical domain. Then, it describes existing approaches for stereoscopic depth estimation using panoramas.

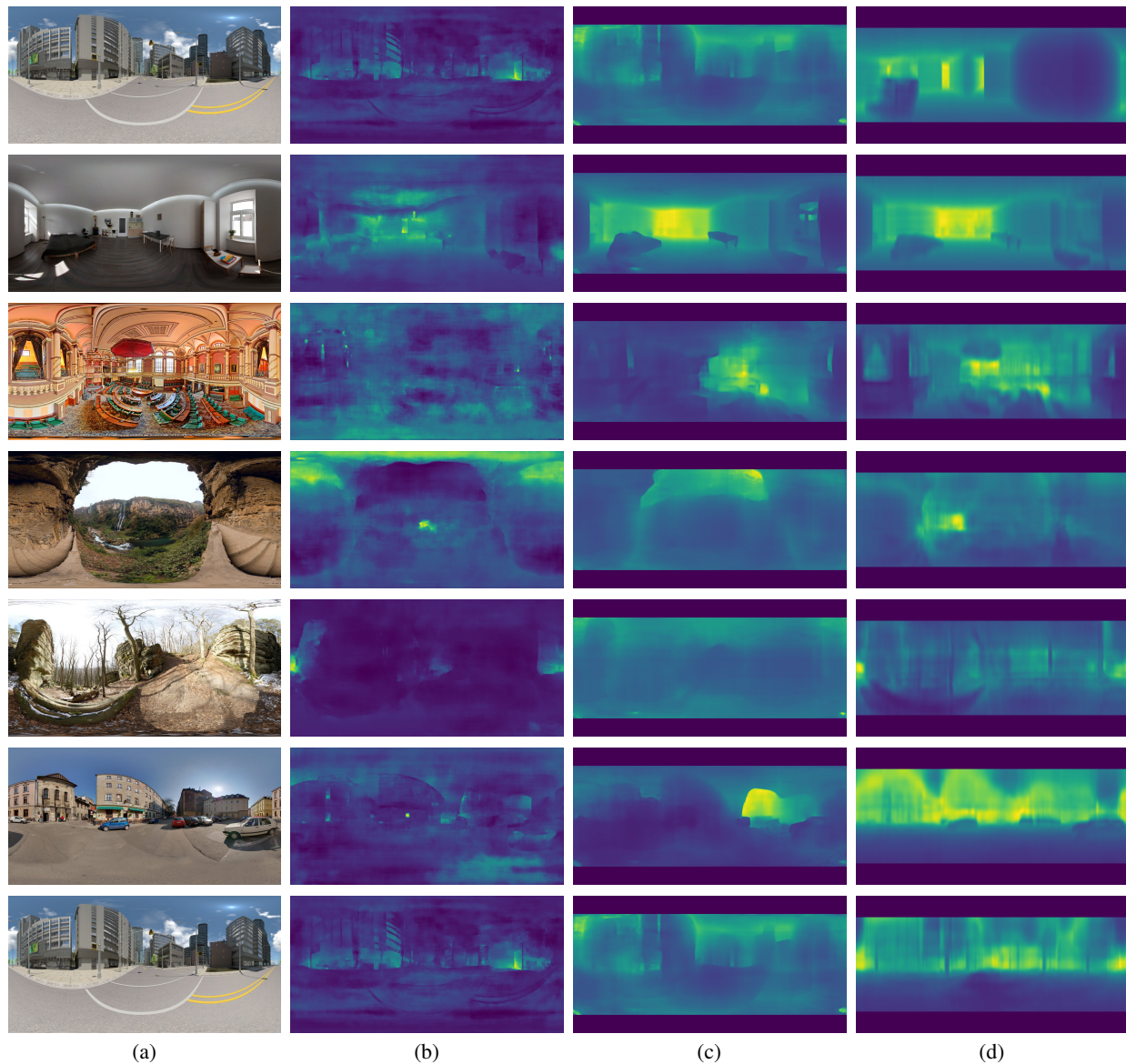


Figure 6: Examples of monocular depth estimation. (a) input color panorama; (b) OmniDepth [118], (c) BiFuse [119], and (d) HoHoNet [115] depth estimates. The first and last color images are available in the 3D60 [118] and Urban Canyon [88] datasets, respectively. The remaining color images were obtained from the SUN360 dataset [84]. Dark blue and yellowish colors represent closer and farther objects, respectively. Depth values are *not* in the same scale. BiFuse and HoHoNet do not estimate depth at the image poles.

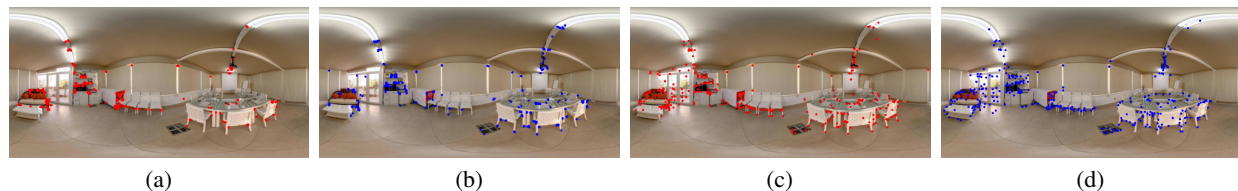


Figure 7: Examples of keypoint detection using planar methods and spherical adaptations. The input panorama, taken from the SUN360 dataset [84], is processed by (a) ORB, (b) SPHORB, (c) SIFT and its (d) spherical adaptation using tangent planes [43].

4.1 Sparse Feature Extraction and Matching

A key problem related to pose estimation and 3D reconstruction is robustly finding correspondence points across two or more views. For that, it is important to find interest points with a well-defined position in the image space that presents stability under image perturbations such as illumination or brightness variations. It is also important to obtain a feature descriptor invariant under various image transformations to perform feature matching among multiple captures of the same scene.

There are many well-known techniques for *planar* keypoint finding and/or description, such as the Harris corner detector [146], Scale-Invariant Feature Transform (SIFT) [147], Affine SIFT (A-SIFT) [148], Speeded Up Robust Features (SURF) [149], Features from Accelerated Segment Test (FAST) [150], Binary Robust Independent Elementary Features (BRIEF) [151], Binary Robust Invariant Scalable Keypoints (BRISK) [152], Oriented FAST and Rotated BRIEF (ORB) [153], KAZE [154], Accelerated KAZE (A-KAZE) [155], among others – a recent survey on planar keypoint matching can be found in [156].

Some works [64, 36, 9] apply planar keypoint algorithms to ERP images of panoramas, which is not ideal since they cannot handle the intrinsic distortions of the spherical camera model [157]. Hence, there has been an increasing interest in keypoint extraction and matching tailored to the spherical domain in the past decade. Cruz-Mota *et al.* [44] adapts SIFT to spherical coordinates (S-SIFT), where the spherical difference of Gaussians is defined. The authors propose to compute both local spherical descriptors and local planar descriptors, so that perspective and spherical images can be matched. To avoid computing the costly spherical Fourier transform, some authors [91, 82, 158, 159] approximate the sphere by a geodesic grid, where a quasi-hexagonal parameterization can be obtained, which allows the adaptation of intensity-based methods. Inspired on the ORB algorithm, Zhao *et al.* [82] propose SPHORB, which explores spherical FAST [158] and adapts BRIEF to the spherical domain using the geodesic grid. In their approach, the grid is stored in distinct a set of triangles with no direct connections, which leads to distortions and special cases on the boundaries of each set. On the other hand, Guan *et al.* [91] use a half-edge data structure to represent the geodesic grid. Then, they use the spherical FAST algorithm as a keypoint detector, and adapt BRISK to the spherical domain, which is named BRISKS. According to [82, 91], these methods outperforms S-SIFT [44] in robustness and repeatability validation metrics under rotation. Further comparison of most previous methods can be found in [157].

All techniques described so far adapt hand-crafted keypoint algorithms to work on the sphere. However, solutions based on deep learning for keypoint matching in perspective images have shown promising results (such as [160]). We are not aware of deep learning-based keypoint extractor/descriptor for panoramas, but one can embed planar deep learning-based approaches through TPP projections of 360° imagery, as recently shown in [43] for planar hand-crafted descriptors.

For the sake of illustration, Fig. 7 shows a comparison of planar keypoint extraction methods and different spherical adaptations. More precisely, Figs. 7(a)-(b) show the keypoints detected with both ORB and SPHORB, and Figs. 7(c)-(d) show keypoints obtained by planar SIFT and its spherical adaptation using tangent planes [43]. Although it is hard to see the differences in a single image, *planar* keypoint matching algorithms suffer from poor repeatability, precision, and recall metrics when applied to spherical image pairs that differ by translation and/or rotation [91, 82, 44]. It means that such standard methods cannot handle the spherical distortions present in wide- or full-FoV images such as CP or ERP. Keypoint matching tends to be more effective in CMP representation, but the keypoints found in each of the six cube faces of an image still need to be matched to those found in the six cube faces of another image. Some works consider padding the cube faces for handling discontinuities in correspondences tracking in CMP videos [28]. As planar methods may not work well with 360° images, they can compromise other tasks such as pose and depth estimation.



Figure 8: Input image pair and the underlying flow estimates (shaded areas highlight the circular padding) computed by DeepFlow [34]. The stereo images differ by translation along the three axes. There is no relative rotation between the captures. The “Classroom model” is available at <https://www.blender.org>.

4.2 Dense Feature Extraction and Matching

Optical flow captures the apparent motion of individual pixels using pairs of still images or video sequences, and often assume small motion and brightness constancy. In particular, dense motion maps are useful for obtaining *dense* correspondences from a pair of images. There are many optical flow algorithms designed to work with perspective imagery (refer to [161] for a recent survey). Similarly to sparse feature matching, some works [41, 162, 64] adopt traditional optical flow approaches for 360° image processing, sometimes in between pre- and post-processing steps. The most straightforward workaround found in literature is to circularly pad ERP images before computing the optical flow, avoiding longitudinal disconnection [41, 162] (recall that a similar strategy was adopted in the context of deep learning for depth or layout estimation, as mentioned in Section 3). Fig. 8 illustrates this strategy for the popular planar *DeepFlow* algorithm [163] as baseline optical flow, used in [41] to obtain dense correspondences for 3D reconstruction.

Mochizuki *et al.* [164] adapts the classical Horn-Schunck algorithm [165] to the spherical domain and applies it to omnidirectional image-based robot navigation. Inspired on [166], the approaches presented in [167, 168] perform a multi-resolution decomposition of the sphere to speed-up the computation of the adapted Horn-Schunck algorithm, estimating motion on the lowest resolution and propagating it to higher resolutions. These approaches, however, tend to fail when high-frequency components of the image are noisy. The strategies presented in [169, 170] use a multi-channel approach that performs convolution with spherical wavelets, achieving a good compromise between computational cost and robustness. In another line of work, Bagnato *et al.* [171], extend the Total Variation L1-Regularized [172] approach for real-time optical flow. However, instead of working on the sphere, they design a graph-based framework (where the vertices represent image pixels and edges define connections between pixels weighted by the geodesic distance) and define the differential operators over these discretization formulas. Kim and colleagues [173] normalize the flow patterns by equalizing optical flow results of pairs of images rotated by 90 degrees on different axes, and then test it in a downstream task (rotation estimation), obtaining improved results when compared to planar methods.

Other authors focus on the adaptation of deep learning-based optical flow algorithms originally designed for planar images to the spherical domain (recall the discussion in Section 3.1). Xie *et al.* [132] integrate DNN layers for spherical adaptation of existing optical flow architectures [174, 175, 176], testing three special layer neural networks: correlation convolution [175], coordinate convolutions [131] and deformable convolution [133]. They report that these layers minimize the error on boundaries on their dataset, named FlowCLEVR dataset. In the same direction, Artizzu *et al.* [177] adapts the *FlowNet* algorithm [175] to the spherical domain implementing a distortion-aware convolution kernel that reuses planar learned weights and architecture. Spherical data is not required for the training procedure. Bhandari *et al.* [178] adapts the *LiteFlowNet* algorithm [179] to the spherical domain by modifying the kernels size depending on the latitude angle of ERP images, and a refinement process that involves a correction factor. These deep learning-based optical flow methods outperform their planar counterparts, but comparisons with other spherical optical flow estimators are still scarce.

4.3 Depth Estimation

Sparse and dense feature matching, revised in Sections 4.1 and 4.2, are often employed in stereo- and multi-view-based methods for 3D geometry recovery. Stereo image pairs are captured under arbitrary translations (as illustrated in Fig. 8) or using fixed baselines – typically horizontal or vertical (as illustrated in Fig. 9). Furthermore, some approaches disregard the rotation component (which might be guaranteed by the capture process using camera rigs or undone when more flexible setups are employed). Most works do not assume specifically indoor or outdoor image pairs as input. Note, however, that the intermediate step of feature matching tends to be more challenging outdoors simply because some objects tend to be too far – occupying only a few pixels. Minimal disparities or triangulations resulting in 3D points too far from the virtual camera can be filtered in a postprocessing step. These procedures, however, are barely stated in most works.

This section discusses stereo matching approaches based on spherical image pairs only, and Table 2 presents an overview of the reviewed techniques. They vary in terms of image representation, employed technology for feature matching

Table 2: 3D geometry estimation methods based on a pair of spherical images.

Reference	Representation	Technology	Matching	Density
Li and Fukumori [57]	HP ($\times 4$)	Triangulation	Keypoints	Sparse
Arıcan and Frossard [180]	ERP	Energy minimization	Pixel-wise	Dense
Kim and Hilton [19]	ERP	PDE-based optimization	Block matching	Dense
Pathak <i>et al.</i> [64, 8]	ERP	Linear/Non-linear optimization	Keypoints/Optical flow	Dense
Pathak <i>et al.</i> [7, 181]	ERP	Linear/Non-linear optimization	Keypoints/Optical flow	Dense
Kim <i>et al.</i> [182]	CMP	PDE-based optimization	Block matching	Semi-dense
Kim <i>et al.</i> [183]	CMP	PDE-based optimization	Block matching	Semi-dense
Wegner <i>et al.</i> [33]	CP	Energy minimization	Block matching	Dense
Lai <i>et al.</i> [123]	ERP	DNN	Learned features	Dense
Wang <i>et al.</i> [184]	ERP	SDNN	Learned features	Dense
Roxas and Oishi [185]	HP ($\times 1$)	Energy minimization	Pixel-wise	Dense

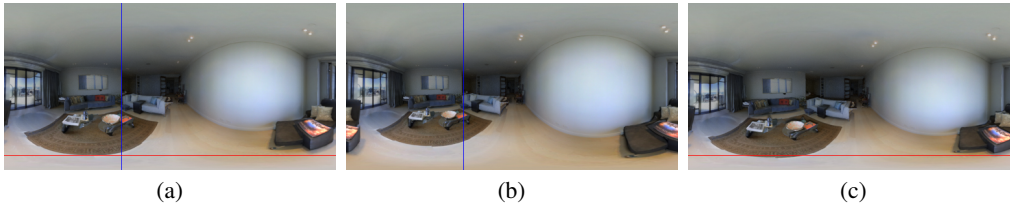


Figure 9: Stereoscopic 360° image pairs. A (a) reference image and two stereo views with (b) horizontal (left to right) and (c) vertical (down to up) baselines (0.26m in both directions). Colored guidelines are drawn for better visualization of the offsets. Source image taken from the 3D60 dataset [118].

and depth regression, and the density of the resulting depth (or disparity or 3D) estimates. Sparse estimates are often associated with sparse feature matching, which might be densified by extrapolating the sparse field. Intrinsically dense methods, on the other hand, provide one depth (or disparity) value for each pixel of the spherical image.

Li and Fukumori [57] were one of the pioneers in stereo-panorama depth estimation. They actually used two pairs of wide-FoV/HP images as source for estimating 3D geometry of scenes, and adapted the main concepts involved in the traditional stereo matching problem to the spherical domain (in fact, they formulated most of what is reviewed in Section 2.1 of this survey). They obtain correspondences in spherical images using the Lucas-Kanade method [186] and enforcing epipolar constraints. Finally, the authors project planar texture patches extracted by a Delanuy triangulation [187] of the sparse point cloud for visualization purposes.

Instead of estimating 3D information based on keypoints, Kim and Hilton [19] introduce a stereo-based algorithm for *dense* 360° disparity estimation. ERP images are created via cross-slits from rotating line-scan cameras with wide-FoV lenses. Then, extrinsic calibration is performed via feature matching. The authors arrange the stereoscopic cameras in a top-bottom configuration so that their epipolar lines are vertically aligned (confer Fig. 9), and introduce a hierarchical partial differential equation (PDE)-based algorithm to estimate continuous disparity maps using the mean-absolute-error/normalized-cross-correlation [188] block matching techniques. Finally, 3D information is estimated via triangulation, and a mesh is built for visualization purposes.

Some authors make the image capture process more flexible. Arıcan and Frossard [180] introduce a method for estimating dense disparities from stereoscopic omnidirectional images in an uncontrolled small baseline. For that aim, they first to rectify both images, so that the epipolar great circles coincide with the longitudes. They formulate a global energy optimization scheme founded in graph-cuts [189] that searches for optimal disparities from a discrete set of possibilities. The authors conclude their paper by presenting hints on how additional cameras can further improve the results. Pathak and colleagues [64, 8] also deal with a setup with small baseline and arbitrary rotation. They first estimate the 5-DoF pose between the two images using A-KAZE features and RANSAC-enabled 8-PA [66], extract the rotation matrix and “derotate” the images. Then, the authors compute dense correspondences using DeepFlow and minimize the moment of the 3D magnitude-normalized flow in an iterative, non-linear manner. When the pose estimate converges, dense 3D information is computed via triangulation. In a follow-up work, Pathak *et al.* [7] opt to process the two images directly on the ERP format, instead of working on the sphere as [64, 8]. According to the authors, this choice helps avoid issues caused by numerical error. The result of the pipeline remains the same as in [64, 8]. This methodology was also published in [181].



Figure 10: Input stereo pair and the underlying depth map estimated using the stereo approach from [123]. Source images taken from a dataset provided by the same authors in [123].

Contrary to most contemporary approaches, Wegner *et al.* [33] work with rotation-free stereo-rectified omnidirectional image pairs represented in a CP format. The authors claim that an approximate formula can be efficiently embedded into existing planar block-matching-based methods for depth inference to be applied to panoramic images. As a proof of concept, they show qualitative results after adapting the cost function of the ISO/IEC MPEG Depth Estimation Reference Software [190] and submitting a pair of stereoscopic images. The disparity/depth estimates on the image poles are poor, and there are apparent seams on both lateral boundaries.

Roxas and Oishi [185] introduce a variational approach for estimating depth from stereoscopic cameras equipped with fish-eye lenses, which does not apply any kind of undistortion or correction and can achieve real-time performance on modern GPUs. The authors propose to use the trajectory field of each pixel involving the baseline, handling multiple correspondences displacement by integrating a coarse-to-fine approach. This strategy constrains the search for matches along the epipolar curves, in a fast way, using linear interpolation. Although their method is applied to HP images, their formulation also applies to any central camera projection.

Recently, some works [123, 184] started tackling the 360° stereo-based depth estimation problem from a learning-based perspective. Wang and colleagues [184] propose an end-to-end deep learning model for regressing disparity from top-bottom stereo 360° images (depth is computed from the disparity maps). The method comprises a two-branch feature extractor that concatenates the stereo pair and polar angle; an Å Trous-Spatial Pyramid Pooling; a learnable cost volume that accounts for the non-linear projection; and an stacked hourglass module for finally estimating the disparity map. The authors claim that using polar angle allows decoupling image appearance from distortion, and show its importance on their ablation study. Lai *et al.* [123] introduce an encoder-decoder network fed with a stereo-rectified pair of ERP images with a small fixed baseline and outputs both depth and normal maps. The authors argue that performing multi-task learning, *i.e.*, also estimating the normal vectors, was paramount for improving the depth estimates. Their main contribution lies in a loss function that encourages associating the left and right boundary information from ERP images. Unlike some geometric-based solutions [64, 8, 181, 7, 180], the learning-based approaches described in [123, 184] are restricted to specific capture setups.

Other methods use additional information to help refine depth estimates based on geometric constraints. Kim *et al.* [182] presented an approach that first produces a depth map based on a pair of vertically-spaced panoramas, and then estimate object and material information for layout recovery with furniture (which requires additional labeled data for training). In the stereo matching, they use a CMP-like projection followed by line detection with the Hough transform to estimate the camera rotations *w.r.t.* the room coordinate system, and then gravity-align the image pair. Correspondences are found using the PDE-based method from [19], and depth information is obtained by triangulation (assuming that the vertical baseline is known). A CNN is used to obtain semantic information about the components, which are combined with the depth map to obtain the furnished room layout. In a follow-up study, Kim and colleagues [183] fuse color image and audio responses for 3D scene geometry recovery. They modify the block world reconstruction method from [182] to accommodate audio and visual data. Visual planes are extracted with the help of superpixels [138], while reflection planes estimated from an omnidirectional microphone array are used during the plane fitting algorithm providing conformal double-source estimates.

Fig. 10 depicts a stereo 360° image pair with fixed horizontal baseline, and the corresponding depth map obtained with [123]. Recall that spherical images capture information along the epipoles – unlike the perspective scenario. Since the epipoles indicate the relative movement direction, it is impossible to effectively estimate depth in that particular region. For horizontal-aligned baselines, the epipoles appear at positions $(\theta, \phi) = (\frac{\pi}{2}, \frac{\pi}{2})$ and $(\frac{3\pi}{2}, \frac{\pi}{2})$. Although the inferred depth map does not present visible artifacts, the original paper [123] indicates missing information around the epipoles when a given recovered 3D scene is visualized as a point cloud.

5 Multi-view 3D Geometry Estimation

Fusing the contributions captured by many views is the core of multi-view-based 3D geometry recovery methods, being pivotal for estimating depth from whole scenarios based on narrow-FoV pin-hole-based images. Panoramas

Table 3: 3D geometry estimation methods based on multiple spherical images.

Reference	Category	Representation	Technology	Matching	Density
Krolla <i>et al.</i> [61]	SLF	CP	Slope estimation	Direct matching	Dense
Gava <i>et al.</i> [83]	SLF	ERP	Energy minimization	Block matching	Dense
Overbeck <i>et al.</i> [191]	SLF	Perspective	Global optimization	Region matching	Dense
Bertel <i>et al.</i> [192]	SLF	Perspective	Camera Interpolation	Optical flow	Dense
Bertel <i>et al.</i> [193]	SLF	ERP	Proxy fitting	Optical flow	Dense
Bagnato <i>et al.</i> [171]	MVS	Graph-based	Global optimization	Optical flow	Dense
Kim and Hilton [19, 194, 16]	MVS	ERP	PDE-based optimization	Block matching	Dense
Kim and Hilton [12, 6]	MVS	CMP	PDE-based optimization	Block matching	Semi-dense
Won <i>et al.</i> [195, 196]	MVS	HP ($\times 4$)	CNN	Learned features	Dense
Torii <i>et al.</i> [197]	SfM	ERP	Non-linear optimization	Keypoint/Loop closure	Sparse
Micusik and Koseckà [198]	SfM	CMP - poles	Markov Random Fields	Key-points/Superpixels	Dense
Barazzeti <i>et al.</i> [199]	SfM	ERP	(Comercial solution)	(Comercial solution)	Dense
Fangi <i>et al.</i> [5]	SfM	ERP	(Comercial solution)	(Comercial solution)	Dense
Bagnato <i>et al.</i> [200]	SfM	ERP	Energy minimization	Optical flow	Dense
Schonbein and Geiger [2]	SfM	Catadioptric ($\times 4$)	Energy minimization	Keypoint/Semi-global matching	Dense
Caruso <i>et al.</i> [201]	SfM	HP ($\times 4$)	Non-linear optimization	Block matching	Semi-dense
Cabral and Furukawa [139]	SfM	ERP	Global optimization	Region matching	Semi-dense
Pintore <i>et al.</i> [202, 203]	SfM	ERP	Linear/Non-linear optimization	Boundary matching	Semi-dense
Pagani and Stricker [36]	SfM	ERP	Non-linear optimization	Keypoint/MVS	Dense
Pagani <i>et al.</i> [9]	SfM	ERP	Non-linear optimization	Keypoint/MVS	Dense
Im <i>et al.</i> [27]	SfM	HP ($\times 2$)	Non-linear optimization	Keypoints/Sweeping	Dense
Guan and Smith [60]	SfM	ERP	Linear/Non-linear optimization	Keypoint	Sparse
Huang <i>et al.</i> [28]	SfM	CMP	Non-linear optimization	Keypoints/Block matching	Dense
Silveira and Jung [41]	SfM	ERP	Linear optimization	Keypoints/Optical flow	Dense
Wang <i>et al.</i> [1]	SfM	CMP	CNN	Learned features	Dense
Won <i>et al.</i> [32]	SfM	HP ($\times 4$)	CNN	Learned features	Dense

provide a full FoV, and although only a pair of captures is enough for geometrically obtaining depth data of the whole surrounding region (and even one capture might suffice when using learning-based approaches), using more cameras is useful for solving occlusion-related issues and may increase the quality of the estimates. In particular, handling occlusions and disocclusions is paramount for implementing fully immersive 6-DoF exploration for recent AR/MR/VR applications [39, 41].

This section divides methods into three categories according to the required image capturing protocol. Sections 5.1, 5.2 and 5.3 review 3D geometry recovery techniques based on spherical light-fields (SLFs), multi-view stereo (MVS) and structure from motion (SfM), respectively. Table 3 summarizes the methods reviewed throughout this section highlighting the main category; the input representation, following the notation used in the previous sections (we also review a method that explores a graph-based representation); the main technology behind each approach; the core idea used for feature matching; and the density of the output. Once again, as in the stereo case, most works do not make any assumptions about the scene’s context, *i.e.*, indoors or outdoors. Exceptions include works that rely on learning-based methods trained on indoor scenarios only.

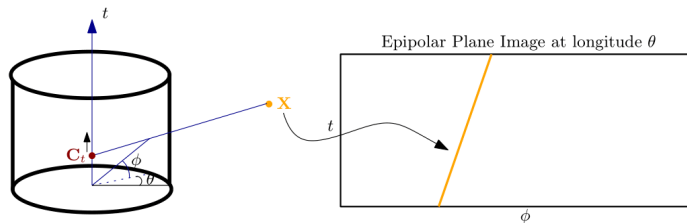


Figure 11: Relationship between SLF, Epipolar Plane Image and depth using a CP model (adapted from [61]).

5.1 Spherical Light Fields (SLFs)

The light field is the representation of the radiance as a function of position and direction, and it can be modeled as a 4D function in the free space as proposed by Levoy and Hanrahan [204]. Such representation resembles the concept of epipolar volumes and planes proposed in [205], which are produced by several closely related captures of a perspective camera along a line and generate directional structures related to depth information. Although using moving cameras is one possibility for estimating the light field, there are other possibilities such as arrays of cameras or cameras with an array of (micro)lenses [206].

For panoramas, earlier approaches for capturing the light field consisted of using a perspective-based light field imaging device coupled with an array of spherical mirrors [207] or rotated in a circular motion pattern [208]. However, the term “spherical light field” was coined in the seminal work from Krolla *et al.* [61], which also presents the first attempts in indoor and outdoor scene reconstruction using full-FoV light fields. They use the Mercator projection [209] to produce CP images from a set of vertically displaced captures. These captures induce Epipolar Plane Images with oriented lines under static scene and Lambertian surfaces assumptions, from which depth can be estimated. Despite the elegant mathematical formulation, the use of CP generates strong distortions around the poles, compromising the depth estimate at these regions. Fig. 11 illustrates the trajectory of a 3D point \mathbf{X} in the Epipolar Plane Image when the camera center \mathbf{C}_t moves vertically. Note that a linear pattern is expected in the $\phi \times t$ plane, and its orientation is related to the depth of \mathbf{X} .

Gava *et al.* [83] propose an approach for tackling SLFs capable of estimating consistent, locally smooth depth values from a scene. Sum-of-squared-differences at the subpixel level helps building a cost volume for each pixel position in a reference view (the central one along the translation axis). A variational approach modeled with data and smoothness terms processes the cost volume and extracts the underlying 3D surface from the scene. Their method extracts sharp depth discontinuities and tackles outdoor scenes, but might fail in textureless areas and occlusions.

Sitzmann and colleagues [210] present a light field representation called Light Field Networks. Similarly to [61], they find an analytical relationship between the directional structures of the Epipolar Plane Images and the scene depth. However, they explore Plücker coordinates to encode the light field instead of a CP representation, which mitigates the limitations around the poles. Despite the promising theoretical results, only simple 3D scenes were explored in [210].

Some approaches explore the concept of SLFs but focusing on other applications such as view synthesis. Although they do not explicitly explore the light field for inferring depth, they make use of multiple camera (or multiple capture) setups to obtain depth information using SfM or MVS approaches. For example, Overbeck *et al.* [191] acquire SLF datasets with two camera rigs: one of them has 16 GoPro Hero4 cameras arranged in a vertical arc placed on a rotating platform (which prioritizes speed), and the other explores a spinning pivoting platform with two Sony a6500 fisheye mirrorless cameras (which prioritize quality). They extract depth information by building a 3D cost-volume and exploring a fast bilateral filtering approach [211], which is used to build a mesh and guide the view interpolation process. Bertel and colleagues [193] used off-the-shelf 360° cameras for the capturing SLFs (typically less than a hundred). Similarly to [191], depth is extracted directly from the captured image set and not the SLF by using a visual simultaneous localization and mapping approach [212].

5.2 Multi-view Stereo (MVS)

The core idea behind MVS methods is to explore three or more *calibrated* cameras for estimating 3D information from a scene. The camera poses can be known *a priori* using a fixed, pre-calibrated camera rig, or obtained on-the-fly using information about the scene. The latter strategy, which demands a more complex camera setup, will be revised in the next section.

A direct way to obtain a dense depth map is to triangulate optical flow-guided correspondences (recall Section 4.2) if the camera poses are known. As an example, Bagnato *et al.* [171] explore this idea, but the details of the depth map might be compromised due to the regularizer used to obtain the optical flow.

Kim and Hilton present incremental solutions for 3D recovery using multiple stereo pairs [19, 194, 12, 16]. In [16] they extend their stereo-based approach described in [19], which was discussed earlier in Section 4. More precisely, a mesh is extracted by triangulation from each cube-map projected disparity map, which is registered with the others through an adaptation of the iterative closest point (ICP) algorithm [213] supplied with surface reliability checking. The combined mesh presents a fair 3D structure with attenuated occlusion-caused issues and well-defined textured regions. Preliminary versions of the work published in [16] can be found in [19, 194]. In [6], they present a light-weight alternative to [16], assuming Manhattan worlds (as done for 3D layout recovery). The authors use the same camera setup as [19, 16], but the images are represented in CMP format after multi-view façade alignment. Initial disparities are estimated by their PDE-based approach [19, 16], and planes are fitted and registered together with the help of SURF features. The resulting planes are refined based on reliability, visibility, and occupancy checks, and finally, the final cuboid representations are built. A preliminary version of [6] can be found in [12].

More recently, Won *et al.* [195] presented an end-to-end deep learning approach for depth map estimation from ultra-wide FoV cameras (four 220° FoV fisheye views). A 2D CNN extracts features that are projected onto spheres with varying radii (sphere sweeping), and a 3D encoder-decoder network builds a cost volume and outputs dense depth panoramas. An extended version [196] further analyzes the inverse depth probability distributions in uncertain regions and proposes a regularization strategy to improve the depth estimates. The results shown in [195, 196] are compelling, but they do not explore other camera setups and disregard calibration camera noise.

As a final comment, we note that a calibrated spherical rig generates a set of six calibrated “semi-planar” views for each spherical image in the rig when the CMP representation is used, which might allow the use of traditional MVS approaches for the individual cube faces. However, the FoV (90°) in each face is higher than most pinhole cameras and leads to a certain level of “radial” distortion [129, 201], which may impact the performance of planar feature detectors [148]. Also, small indoor scenarios and captures where the camera is too close from a wall may result in cube faces with practically no texture, so that feature matching and further depth recovery tend to fail [63]. Moreover, spherical captures presenting rotations generate CMP images that are not aligned – the faces in one capture might relate to a region comprising two or three faces in other captures – which might highlight distortions. As such, it is advisable to perform image derotation [140, 80] on the sphere before generating the CMP images, or to explore camera setups with small rotations as in [19, 194, 12, 16], which assume upright image captures. Finally, per-face depth estimation tends to produce discontinuities along face edges [87, 119, 32], and post-processing is required to obtain the full 3D model of the scene. Despite the stronger distortions present in ERP representations, we believe that they present more potential for exploring global information through deep learning approaches as in [195, 196], particularly if coupled with spherical network adaptations as presented in Section 3.1.

5.3 Structure from Motion (SfM)

SfM aims to estimate camera poses and the 3D structure of the scene. If camera poses are known, 3D reconstruction can be achieved using MVS, as described in Section 5.2. SfM is often called visual simultaneous localization and mapping (V-SLAM) in the robotics jargon, with the additional constraint of online processing [56]. We add that V-SLAM usually explores temporal information (robot-mounted camera exploring an environment) and focus mostly on the camera pose (trajectory) part of the problem, whereas our goal in this survey is 3D geometry recovery.

The problem of reconstructing large 3D outdoor scenes using a single moving omnidirectional camera was tackled in [197, 198, 201]. Torii *et al.* [197] and Micusík and Koseckà [198] use planar SURF descriptors to obtain correspondences across frames, but trajectory estimation exploring loop closure (as in other approaches for V-SLAM) was the focus in [197], whereas depth estimation (with the help of superpixels, under a piece-wise planar assumption) was the main goal of [198]. Caruso *et al.* [201] explore a robust photometric error to align the frames and explore keyframe matching to refine the alignment. A semi-dense depth map is then obtained by direct search over epipolar curves. The main goal of [197, 201] is motion/trajectory estimation, and only a visual analysis is provided for the obtained 3D data; the method from Micusík and Koseckà [198] provides a denser reconstruction, but since it is based on planar primitives, it is not able to capture finer scene details. Huang and colleagues [28] also explore a moving camera, but targeting indoor scenes and view synthesis applications for VR. They track features using Kanade-Lucas-Tomasi (KLT) [186] in regularly sampled CMP keyframes, and explore a bundle-adjustment (BA) procedure for incrementally refining both the camera pose and sparse 3D estimates. They further adopt an algorithm based on normalized-cross-correlation [214] that generates a dense depth map via interpolation of the sparse 3D points of each keyframe. Finally, the method merges all the depth maps and creates a mesh representation suited for 3D rendering. Despite the promising view synthesis results shown in [28], large camera displacements across adjacent frames might compromise KLT tracking. It is also worth

mentioning the OpenVSLAM framework [212], which can handle several camera types including panoramas. However, since planar ORB features are used for matching, the tool does not fully explore the potential of spherical imagery.

The works of Barazzeti *et al.* [199] and Fangi *et al.* [5] targeted larger scenes in the context of cultural heritage, but focused on the evaluation the 3D error of spherical SfM approaches using different cameras. A consumer-grade Samsung Gear 360 camera was analyzed in [199], whereas a high-resolution Panono 360° camera was evaluated in [5]. Although not many technical details about the underlying SfM approaches were provided in either work (they use a commercial solution), they both reported low reconstruction errors, highlighting that non-uniform illumination was a challenge for capturing indoor panoramas.

Other works focus on the estimation of denser 3D maps. Bagnato *et al.* [200] explore their spherical optical flow approach [171] to obtain dense correspondences, which is integrated with an ego-motion estimator in an alternating fashion. Unlike [171], it does not require the camera trajectories to be known, but it suffers from the same drawbacks of [171]: problems with large displacements (due to linearization of the flow) and loss of details for small objects. Schonbein and Geiger [2] also target at dense 3D reconstruction assuming augmented Manhattan worlds. The authors explore a moving rig of four calibrated catadioptric cameras so that MVS can be used for spatial and SfM for temporal alignments. They match planar descriptors (a combination of FAST and BRIEF) for motion estimation, and use it to rectify the four omnidirectional stereo pairs. Depth is recovered through a spherical semi-global stereo matching algorithm, in which planar hypotheses are obtained by a Hough-like voting scheme applied to a superpixel representation of the (inverse) depth map and combined in a discrete energy minimization problem. Their approach presents fair results, but requires a pre-calibrated rig and is computationally expensive. Pagani and Stricker [36] propose a pipeline with two phases: (i) an SfM step for recovering the pose and sparse 3D representation of the scene; and (ii) an MVS step for estimating denser representations of the scene. More precisely, they use ASIFT-like keypoints and an 8-PA RANSAC framework, followed by non-linear optimization, for pose recovery. A sparse point cloud is obtained by iteratively solving the perspective-n-point (PnP) problem via direct linear transform (DLT) [69] and applying a non-linear camera pose refinement. Finally, a densification process explores the popular Patch-based Multiple View Stereo (PMVS) algorithm [215]. A similar work [9] also explored PMVS, but using a more systematic approach for finding anchors to guide PMVS. Both approaches present compelling visual results, but no comparison with other techniques is provided.

Specific properties of panorama capture devices can also be used for SfM. Im *et al.* [27] explore weakly overlapping fisheye sensors looking at opposite directions from short, narrow-baseline monocular 360° videos. Due to the small motion assumption, the authors directly minimize the reprojection error on the unit sphere using Harris corner features that are tracked by the KLT algorithm [186]. They also propose a sphere sweeping algorithm (extending the main idea behind traditional plane sweeping) that generates a dense depth map from the video. Besides being dependent on a dual wide-FoV fisheye sensor and short slow motion videos, their method tends to produce noisy 3D reconstructions due to the lack of a regularizer.

Guan and Smith [60] address the 360° video stabilization problem via SfM. They match sparse S-SIFT features across frames, and use the 8-PA supplied with RANSAC to estimate the initial two-view camera pose. Additional camera poses are estimated by solving the PnP (renamed to ‘Spherical-n-Point’, or SnP) problem via DLT. The main contribution of [60] is the introduction of a BA framework that is optimal for the assumed noise model for keypoint matching errors on the unit sphere, based on the von Mises-Fisher distribution [216]. The low pose estimation errors achieved by their method may indicate good results in 3D reconstruction, but dense geometry recovery is not addressed in their work. Silveira and Jung [41] followed a similar approach for pose estimation, but aiming dense reconstructions. They used sparse SPHORB features to solve the two-view camera poses (via 8-PA-RANSAC) relating one reference view to all others. The rotation parameters extracted from the Essential matrices are used to align (derotate) all views (similarly to [198]), and DeepFlow was used to obtain dense correspondences between the reference image and the remaining aligned views (circular horizontal padding was used). The full translation vectors of all views are obtained using a simplified SnP model, and a weighted multi-view calibrated reconstruction yields a dense depth map, further post-processed with a spherically-modified Domain-Transform filter [217]. As an illustration, Fig. 12 shows a reconstruction result using [41] based on nine input panoramas.

A set of approaches focus on indoor 3D scene reconstruction assuming Manhattan worlds [139, 202, 203]. Cabral and Furukawa [139] claim to use a traditional SfM scheme to find the camera poses (no details are provided) and MVS to obtain 3D point clouds, which are combined with an oversegmented representation [138] of each panorama to obtain an initial labeling as wall, floor or ceiling. A 2D floorplan is built using a graph-based approach, and the final 3D model is obtained by extruding the walls up to the ceiling. Pintore and colleagues [202, 203] also explored superpixel-based classification primitives, but using Simple Linear Iterative Clustering (SLIC) [218] instead. While the work in [202] strongly relies on SfM for obtaining 3D information, the approach in [203] focuses on independent single-image layout reconstruction (recall Section 3.2), and explores multi-view alignment (using the BA approach for CMP representations presented in [219]) mostly for refining the per-image layouts and obtaining the multi-room

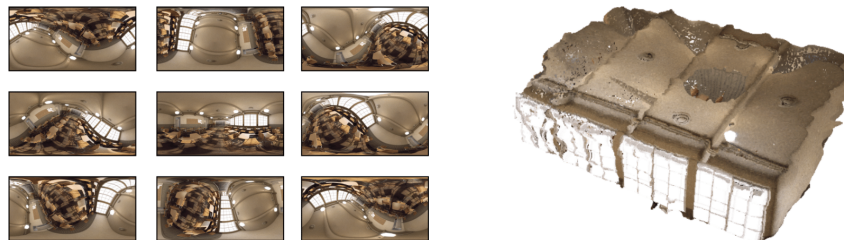


Figure 12: Multiple views and the underlying recovered 3D geometry using the SfM approach from [41]. The “Class-room model” is available at <https://www.blender.org>.

reconstruction. Note that these three approaches explore superpixels designed for planar images, which might lead to an undesired over-segmentation around the poles (due to the non-uniform sampling of panoramas), which could be replaced with superpixel algorithms tailored to the spherical domain such as [220, 221, 222].

In the direction of deep learning, Wang *et al.* [1] present a self-supervised approach for spherical SfM. Their model uses CMP images and treat each cube face as planar (with a special treatment at the edges of the cube). Two networks (one for depth and the other for camera motion estimation) work on each individual cube face, and then are combined to incorporate photometric and pose constraints exploring relative (known) pose differences among the faces. Won *et al.* [32] also tackle both the pose and 3D scene reconstruction problems, but by considering four fisheye cameras spaced by a wide and fixed baseline. Intrinsic camera calibration is a requirement for fisheye imagery (performed offline), and a BA algorithm handles the extrinsic calibration. The authors introduce a CNN model that takes warped fisheye images and outputs a cost volume that is filtered using a sweeping method and further aggregated by semi-global matching. Although the authors argue that the method works with full spheres, they disregard the image poles in their evaluation. In a follow-up study [223], they modify the CNN and add a loop-closure detection module, improving both pose and 3D reconstruction estimates.

6 Benchmarking: Datasets and Evaluation Metrics

All approaches surveyed in this paper address the problem of inferring 3D information from a scene. However, the representation can be encoded as layout corners, sparse point clouds, dense point clouds, set of planar patches, or even meshes. Moreover, some methods present metrical depth estimates while others use a fictional distance (particularly for single-panorama methods). As such, comparing this diversified set of approaches is not an easy task. Next, in Sections 6.1 and 6.2, we compile and briefly describe relevant datasets and figures of merit used to assess all these kinds of techniques. Finally, we show selected state-of-the-art results considering common datasets and figures of merit for the tasks of single-image layout and depth estimation in Section 6.3.

6.1 Datasets

An increasing number of datasets contain annotated panoramas for 3D reconstruction applications. A list of representative datasets, categorized *w.r.t.* the information they provide, is shown in Table 4. The next subsections briefly describe these datasets, indicating if they are mostly suited for the layout or depth estimation problems.

6.1.1 Layout Estimation

Dataset from [137] – Zhang and colleagues [137] select 700 ERP images of scenes including bedrooms and living rooms from the SUN360 database [84], which has about 57,000 different full-FoV color images taken in both indoor and outdoor scenarios. The dataset from [137] provides the 3D bounding volume annotations for the scene layout and the objects therein. The layouts are modeled as simple cuboid shapes. Two halves compose the train and test data.

Dataset from [4] – Fernandez-Labrador *et al.* [4] provide layout annotations to a subset of the SUN360 [84] and Stanford 2D-3D [145] datasets, yielding 518 1024 × 512 ERP images and annotated layout borders and corners, provided as probability maps. Annotated layouts are assumed to fit the Manhattan world assumption. Train and test splits are preset.

Dataset from [109] – Zou *et al.* [109] provides cuboid layout annotations for 571 images taken from the Stanford 2D-3D [145] dataset. Layout annotations are given as 2D layout corners in ERP format. Train, validation, and test splits are provided.

Table 4: Publicly available 360° imagery datasets.

Reference	Dataset URL	Number of Images	Data Source	Annotation Type
Zhang <i>et al.</i> [137]	http://panocontext.cs.princeton.edu	700	Subset of [84]	Layout
Fernandez-Labrador <i>et al.</i> [4]	http://webdiis.unizar.es/~jmfacil/cfl/sun360	518	Subset of [84]	Layout
Zou <i>et al.</i> [109]	https://github.com/zouchuhang/LayoutNet	571	Subset of [145]	Layout
Yang <i>et al.</i> [95]	https://github.com/SunDaDenny/DuLa-Net	2,573	Subset of [84]/Original	Layout
Pintore <i>et al.</i> [111]	https://github.com/crs4/AtlantaNet	122	Subset of [224, 225]/Original	Layout
Armeni <i>et al.</i> [145]	http://3dsemantics.stanford.edu	1,413	Original	Depth, normals, semantics, and camera poses
Chang <i>et al.</i> [225]	https://niessner.github.io/Matterport/	10,800	Original	Depth, semantics, and camera poses
Zioulis <i>et al.</i> [118]	https://vc13d.github.io/3D60/	24,933	Re-renderings from [225, 145, 226]	Depth and normals
Wang <i>et al.</i> [1]	https://fuenwang.ml/project/360-depth/	25,000	Re-renderings from [226]	Depth and camera poses
Tchapmi and Huber [227]	https://sumochallenge.org/	58,631	Re-renderings from [226]	Depth, semantics, and camera poses
Zheng <i>et al.</i> [224]	https://structured3d-dataset.org/	196,515	Original	Layout, depth, normals, albedo, instance, semantics, and camera poses
Lai <i>et al.</i> [123]	https://github.com/pokonglai/ods-net	50,000	Re-renderings from [145]	Depth and normals
Wang <i>et al.</i> [184]	https://albert100121.github.io/360SD-Net-Project-Page/	3,577	Re-renderings from [145]	Depth and disparity
Won <i>et al.</i> [196]	http://cvlab.hanyang.ac.kr/project/omnistereo/	2,560	Original (Blender Scenes)	Depth
Jin <i>et al.</i> [116]	https://svip-lab.github.io/dataset/indoor	1,755	Original	Layout and depth

Realtor360 dataset – Yang and colleagues [95] provide layout annotations (4 to 12 corners) for 593 panoramas from a subset of the SUN360 database [84]. The authors also annotate 1,980 360° images from a real estate database. The annotated data models Manhattan world scenarios. Train and test splits are provided, and the dataset might be available upon request.

AtlantaLayout dataset – Pintore *et al.* [111] annotate 122 ERP images of variable size (*e.g.*, 512×1024 , 2048×1024 , 5376×2688) from different sources, such as Matterport3D [225] and Structured3D [224]. The annotations are provided as 2D ERP coordinates corresponding to 3D corners of Atlanta world scenarios. Train, validation and test splits are provided.

6.1.2 Depth/3D Estimation

SUNCG – Song *et al.* [226] provide 45,622 computer-generated 3D scenes with semantic information suitable for rendering. The SUNCG dataset does not provide panoramic images, but it is used in related literature. A method for simulating real depth captures is also made available.

Stanford 2D-3D – Armeni *et al.* [145] made available more than 1,413 full-FoV indoor real captures from six large-scale areas, including offices, classrooms, and corridors. The dataset offers registered depth, normals, and semantic

maps. Color information is, however, missing in the poles. The camera poses, point clouds and 3D meshes are also available. Train and test splits at the area level are preset.

Matterport3D – Chang *et al.* [225] provide 10,800 panoramic views from 90 real building-scale scenarios. The images are in CMP format and cover 3.75 steradians (poles are missing). The dataset also provides depth, camera poses and semantic segmentation information. Train, validation, and test splits are made available at the scenario level. Manhattan layout annotations were recently added to a subset of Matterport3D by [49].

3D60 – Zioulis *et al.* [118] made available 24,933 512×256 ERP-formatted renders from other datasets: Matterport3D [225], Stanford 2D-3D [145], and SunCG [226]. It contains aligned color, depth, and normal maps in a trinocular camera setup. Train and test splits are preset.

PanoSUNCG – Wang *et al.* [1] provide about 25,000 images captured from 103 different scenarios from SUNCG [226] in five camera paths. The dataset provides the color, depth and rendering trajectory. The authors suggest using data from 80 scenes for training and the remaining 23 for testing.

Scene Understanding and Modeling (SUMO) – Tchapmi and Huber [227] made available 58,631 computer-generated indoor CMP images from the SUNCG dataset [226]. Each cube face has 1024×1024 pixels. Camera poses, depth, and 2D/3D semantic information are also provided.

Structured3D – Zheng *et al.* [224] provide 196,515 frames from 3,500 synthetic, photo-realistic house designs. A scene has 1024×512 ERP images at three different light conditions and camera poses. Instance annotation, semantic, albedo, normal, layout, and depth maps are available. The dataset also enables object detection, scene understanding, and view synthesis.

Dataset from [123] – Lai and colleagues [123] make available a re-rendered subset of the Stanford 2D-3D [145] dataset along with ground truth for depth and normal maps. Namely, the authors provide about 50,000 256×128 stereoscopic ERP images separated by a horizontal baseline of 6.5cm. Depth values are given in meters. Train and test splits are provided.

Dataset from [184] – Wang *et al.* [184] make available a re-rendered subset of the Stanford 2D-3D [145] and Matterport3D [225] datasets. It contains 3,577 1024×512 stereoscopic ERP image pairs separated by a vertical baseline of 20cm. Depth and disparity maps are also made available. Train, validation, and test splits are provided.

Datasets from [196] – Won *et al.* [196] provide three wide-FoV synthetic video-sequences rendered with Blender [228]. There are three scenarios: one outdoors and one indoors. A total of 2,560 frames are made available. Depth information is provided. Train and test splits at video-sequence level are preset.

Shanghaitech-Kujiale dataset – Jin *et al.* [116] provide a synthetic dataset containing two 1024×512 ERP images for 1,775 rooms – with and without furniture. The dataset also has depth maps and room layout (corners and edges) annotations. Train and test splits are provided.

In general, datasets with preset train, validation, and test splits allow a fair and reproducible comparison among different techniques. For the layout case, simpler annotations (such as cuboids) can be used for (pre-)training and assessing more general approaches (such as those dealing with Manhattan or Atlanta worlds [109, 111]), but without exploring their full potential. On the other hand, methods that assume more constrained layouts cannot be trained or tested using datasets with generic annotations without a proper conversion. Note that datasets proposed exclusively for layout estimation still have a limited number of images. Many datasets are used for monocular depth benchmarking, such as the Matterport3D, Stanford 2D-3D, and the 3D60 – which unites the two former plus re-renderings from the SUNCG. Only few datasets consider captures from multiple views to be used for stereo- or multi-view-based depth estimation, such as 3D60, PanoSUNCG, and the datasets from [123, 184, 196]. More generic datasets, such as the SUMO, Structured3D, and Shanghaitech-Kujiale datasets have much more data, are applicable to both monocular layout and depth estimation, but contain only synthetic scenarios.

6.2 Evaluation Metrics

A plethora of figures of merit can be used to assess the quality of a 3D scene geometry reconstruction method. Next, we point out the most popular metrics found in the literature, distinguishing approaches suitable for layout from those for depth/3D geometry estimates.

6.2.1 Layout Estimation

Layout information can be represented by corners or edges, which can be considered as (possibly binarized) probability maps lying on the 2D or 3D space. Classical metrics like precision, recall, F1-score, and accuracy can be applied to layout estimates – represented either as corners or edges – when formatted in an ERP image [104, 4, 108]. Additionally,

the intersection over union (IoU) can be applied to both ERP images (2D IoU) [111, 95, 4, 115] or data (back)projected to the 3D space (3D IoU) [111, 224, 109, 95, 4, 110, 108, 115]. Angular corner error and object/planar surfaces length/area disagreement are also used for assessing scaled layout estimates [106, 105].

More specific metrics are also found in the literature. The corner error (CE) computes the normalized L2 distance between the predicted and ground truth corners [111, 224, 109, 4, 110, 108]; and the pixel error (PE) – or pixel classification error (PCE) – measures the pixel-wise error between predicted and ground truth surface (plane) classes of the cuboid representation [111, 102, 224, 109, 4, 110, 108]. The equally oriented pixel ratio (EOP) [107, 103] computes the percentage of pixels in a predicted label map representing the walls/floor/ceiling orientations that match the ground truth (a simplified normal map-like with three classes only).

6.2.2 Depth/3D Estimation

Most methods evaluate depth or 3D estimates after scale correction/alignment (*e.g.*, via mean [114] or median normalization [118, 35]) *w.r.t.* the ground truth annotations. In the monocular depth estimation case, absolute depth values are difficult to obtain. Hence, many authors follow the guidelines proposed by Eigen *et al.* [97, 141], introduced for perspective cameras, which include the accuracy (Acc / δ) at a preset threshold (acceptable error) [123, 6, 27, 118, 185, 115, 100, 35, 93, 119, 32, 195], where δ is a suitable error metric; the mean absolute relative error (Abs Rel / Rel) – or mean relative error (MRE) – [115, 119, 123, 118, 100, 35, 30, 93, 41]; the mean square relative error (Sq Rel) [118, 100, 35, 93]; the linear root mean square error (RMS / RMSE) [184, 37, 6, 123, 16, 195, 118, 115, 100, 30, 119, 32], the logarithmic root mean square error (RMSLE / RMSLog) [37, 118, 115, 100, 35, 30, 119], and the log, scale-invariant mean square error (SIMSE / RMSE log, scale-invariant MSE) [87, 93].

Other common metrics include the L2 [113] and cosine distances [113, 114], the mean square error (MSE) [180], and the mean absolute error (MAE) [61, 184, 6, 16, 83, 195, 19, 185, 115, 119, 32] between estimates and ground truth annotations. Similarly to the accuracy, the completeness (Com) indicates the percentage of the estimates that cover the ground-truth [6, 185]. Although most metrics work on 2D disparity/depth maps, some are considered for assessing 3D representations such as point clouds and meshes [6, 16, 19]. It is also worth mentioning that some methods also disregard part of the obtained estimates (missing renders, poles, etc.) when computing these metrics, such as in [118, 87, 184, 195, 196, 41].

6.3 Selected State-of-the-Art Results

This section compiles state-of-the-art results for the problems of layout and depth estimation using a single spherical image. Throughout this manuscript, the reader can observe a growing trend among researchers and the industry for tackling these ill-posed problems via deep learning, whereas the number of recent stereo- and multi-view-based approaches is not very abundant.

Table 5, adapted from [110] and [112], presents state-of-the-art results for layout estimation under the Manhattan world assumption, which is the most common constraint. Listed results consider the PanoContext [225] and Stanford 2D-3D [145] datasets and the CE, PE, and 3D IoU figures of merit. To the best of our knowledge, DuLa-Net v2 [49] and Single-Shot Cuboids [112] attain the best results up to now.

Table 6, adapted from [115] and [120], shows state-of-the-art results in single-image depth estimation. The results are organized by dataset: Matterport3D [225], Stanford 2D-3D [145], 3D60 [118], and PanoSUNCG [1]. Each dataset listed is used for training and testing, using the suggested preset splits. The estimates are assessed using the MRE, MAE, RMSE, RMSLE and accuracy metrics. Up to this point, to the best of our knowledge, UniFuse [120] and HoHoNet [115] achieve the best results in most relevant datasets.

We conclude this section by reminding the reader that qualitative results, including some of the methods shown in Tables 5 and 6, can be seen in Figs. 5 and 6.

7 Conclusions and Future Trends

Throughout the manuscript, we identified approaches targeting at applications based on room layouts (3D corners or edges of indoor scenes) or explicit depth estimates, which might be either sparse or dense. The revised techniques face this fundamental problem relying on a single, two, or multiple 360° captures. The latter camera setup further divides into light fields – in which the original formulation assumes a very specific camera setup with small baselines in between the cameras and static scenes –, multi-view stereo – which alleviates such constraints but often require manual camera calibration –, and structure from motion – that infers camera poses and 3D geometry from the image sequences

Table 5: State-of-the-art Results in Monocular Layout Estimation.

Dataset	Method	Evaluation Metric		
		CE (%)	PE (%)	3D IoU (%)
PanoContext	PanoContext [137]	1.60	4.55	67.23
	LayoutNet [109]	1.06	3.34	74.48
	DuLa-Net [95]	N/A	N/A	77.42
	Corners for Layout [110]	0.79	2.49	78.79
	HorizonNet [110]	0.76	2.20	82.17
	HorizonNet* [110]	0.76	2.22	81.30
	LayoutNet v2* [49]	0.63	1.79	85.02
	DuLa-Net v2* [49]	0.82	2.54	83.41
	Single-Shot Cuboids [112]	0.53	1.65	84.89
	AtlantaNet [111]	N/A	N/A	78.76
	LED ² -Net [117]	N/A	N/A	82.75
Stanford 2D-3D	LayoutNet [109]	1.04	2.70	76.33
	DuLa-Net [95]	N/A	N/A	79.36
	HorizonNet [110]	0.71	2.39	79.79
	HorizonNet* [110]	0.78	2.65	80.44
	LayoutNet v2* [49]	0.71	2.04	84.17
	DuLa-Net v2* [49]	0.66	2.43	86.45
	Single-Shot Cuboids [112]	0.56	1.83	85.16
	AtlantaNet [111]	0.70	2.25	82.43
LED ² -Net [117]	N/A	N/A	83.77	

Results considering the ResNet-34 architecture [49].

Table 6: State-of-the-art Results in Monocular Depth Estimation.

Dataset	Method	Evaluation Metric						
		MRE	MAE	RMSE	RMSLE	$\delta < 1.25$	$\delta < 1.25^2$	$\delta < 1.25^3$
Matterport3D	OmniDepth* [118]	0.2901	0.4838	0.7643	0.1450	0.6830	0.8794	0.9429
	BiFuse [119]	0.2048	0.3470	0.6259	0.1134	0.8452	0.9319	0.9632
	UniFuse [120]	0.1063	0.2814	0.4941	0.0701	0.8897	0.9623	0.9831
	HoHoNet [115]	0.1488	0.2862	0.5138	0.0871	0.8786	0.9519	0.9771
Stanford 2D-3D	OmniDepth* [118]	0.1996	0.3743	0.6152	0.1212	0.6877	0.8891	0.9578
	BiFuse [119]	0.1209	0.2343	0.4142	0.0787	0.8660	0.9580	0.9860
	UniFuse [120]	0.1114	0.2082	0.3691	0.0721	0.8711	0.9664	0.9882
	HoHoNet [115]	0.1014	0.2027	0.3834	0.0668	0.9054	0.9693	0.9886
	Jin <i>et al.</i> [116]	0.1180	N/A	0.4210	N/A	0.8510	0.9720	0.9860
3D60	OmniDepth [118]	0.0931	0.1706	0.3171	0.0725	0.9092	0.9702	0.9851
	BiFuse [119]	0.0615	0.1143	0.2440	0.0428	0.9699	0.9927	0.9969
	UniFuse [120]	0.0466	0.0996	0.1968	0.0315	0.9835	0.9965	0.9987
PanoSUNCG	OmniDepth [118]	0.1143	0.1624	0.3710	0.0882	0.8705	0.9365	0.9650
	BiFuse [119]	0.0592	0.0789	0.2596	0.0443	0.9590	0.9838	0.9907
	UniFuse [120]	0.0485	0.0765	0.2802	0.0416	0.9655	0.9846	0.9912

OmniDepth is trained with batch normalization for better convergence.

(including but not limiting video footage). As for many other visual computing areas, the scientific community is focusing on modeling the 3D scene geometry recovery problem as a learning problem, achieving impressive results.

As the reader can see throughout this paper, a current trend is to explore a single spherical image for estimating either the layout (of indoor scenes) or explicit depth information. In most scenarios, this camera setup is certainly the most attractive, since there is no need to pre-calibrate cameras and/or take multiple captures of the environment, and even panoramas captured in the past can be used for layout/depth estimation. 3D layout estimation methods often assume different geometric constraints for modeling the scene: cuboid shape, Manhattan, and Atlanta worlds, in increasing order of layout flexibility. Only few approaches for layout recovery rely on unconstrained scene models. However, one may note that the vast majority of indoor rooms do follow simpler geometrical rules (such as cuboid and Manhattan), and consequently most datasets used to train layout estimation models contain mostly these types of rooms. Hence, more complex datasets are required to further explore the potential of more generic techniques (such as Atlanta or even unconstrained scenarios).

Single-image-based depth estimation techniques provide richer information (typically a dense map with the depth value at each pixel), enabling the discrimination of other objects (such as furniture in the case of indoor scenes or the overall scene geometry in outdoor captures). However, as mentioned throughout the manuscript, full (geometrically-consistent) 3D representations of the scenes, such as for immersive navigation in AR/MR/VR applications, require complementary information from additional supporting views for addressing occlusions and disocclusions that appear when the (virtual) camera position changes, and also to obtain *truly* geometrical 3D information. Therefore, robust multi-view approaches should still be the focus of attention of several research groups worldwide. Hybrid solutions may combine multiple single-view depth estimates from the same scene in a multi-view scene completion framework.

The increasing popularity of learning-based solutions raises the need for large annotated datasets (or 3D synthetic data that can be rendered using virtual spherical cameras). In fact, the number of publicly available datasets has been increasing in the past years (see Table 4 for a summary). However, they still contain a limited variability (e.g. mostly indoor environments or indoor scenes with a certain type of room geometry). Fig. 6 illustrates the well-known data-dependence issue, but in the context of depth estimation. Note that results for “unusual” indoor and outdoor scenes are considerably worse than those for indoor scenes. In fact, only two revised works mentioned the possibility of estimating depth from a single image taken in outdoor scenarios. A possible trend to mitigate the lack of annotated data is to rely on knowledge distillation, where inter-domain transfer learning techniques can be applied for taking advantage of consolidated perspective datasets in problems with scarce spherical data.

A related issue concerns the definition of standardized figures of merit for quantitative assessment, which would allow a fair comparison among different approaches. There is still no consensus in the literature about how to establish a benchmark evaluation setup that encompasses all competing approaches, but the release of publicly available code by the authors – which fortunately has been an increasingly popular procedure – is a good sign. In particular, we believe that both the problems of dataset availability and definition of standardized quantitative assessment metrics is even more challenging for the stereo- and multi-view-based scenarios, since they required more than one capture for the scenarios, and the ground-truth annotations must refer to a reference capture. However, the existence of standardized datasets and benchmarks for stereo-related problems using perspective images such as Middlebury [24] and KITTI [229] can inspire the creation of spherical counterparts to deal with panoramas.

One aspect that is transversal to all topics tackled in this paper is the chosen representation for the spherical image. On the one hand, the CMP representation provides six planar views of the scene that resemble the outputs of perspective cameras, which is a reasonable choice if we want to explore the vast arsenal of tools that is already available for perspective images. We believe that such representation is suitable for applications such as pose estimation in stereo or multi-view setups since methods for keypoint detection, description, and matching devised (or trained) for perspective images could be used with some adaptations – Section 5.2 provides a few insights in the context of MVS. Since CMP faces still present wider FoVs than a typical pinhole camera, an alternative to alleviate the distortions in the spherical-to-planar mappings can be the use of local tangent plane representations, such as the approach presented by Eder and colleagues [43]. In fact, the adaptation of the planar SIFT descriptor using local tangent planes was shown in [43] with promising results. On the other hand, we believe that the ERP is a more suitable choice for methods that explore deep neural networks, which is usually the case for single-image layout or depth estimation. In these applications, the receptive field of convolutional layers is implicitly enlarged with the pooling layers, allowing the network to learn progressively more global information. Since the ERP provides all the information in a single image, it allows the exploration of all image content in the network. In fact, recent methods that have shown state-of-the-art results such as [110, 115] propose non-local propagation of information over the horizontal direction of the ERP image using recurrent layers. Performing analogous data propagation schemes in CMP representations require adequate stitching of the cube faces, and our literature review shows that single-image layout or depth estimation methods use mostly CMP in conjunction with ERP [119, 120].

We could also perceive an increasing interest in developing deep neural networks that take into account the inherent deformations of spherical images regardless the representation, as shown in Section 3.1. However, these models are still considerably slower than traditional planar deep neural networks, and the use of spherically-adapted networks is still not a consensus at least in layout/depth estimation applications. Not only end-to-end approaches for 3D geometry recovery are expected to emerge, but also relevant geometrically correct learning-based tools for dealing with sparse and/or dense matching, plane-aware image oversegmentation, pose estimation, etc., should be developed in the near future.

Last but not least, we understand that there are still some challenges to be overcome in terms of technical development and applications. Single-panorama layout estimation of a room with simplified geometry presents quite mature solutions and may allow virtual tours in real estate applications, but recovering more complex geometry and fined 3D structures (e.g., furniture) is still ongoing research. Contextual information may preclude several applications that depend on learning-based methods, such as for single-image depth inference. Allowing the estimation of a wide range of depth values for outdoor scenarios, for instance, may impact the parametrization of the networks and demand unavailable data. Estimating depth in a single frame fashion from video footage may generate flickering due to the lack of temporal coherence. Single and multi-view approaches can be coupled to allow full 6-DoF immersive navigation. Applications such as robot navigation and infrastructure inspection need to build a scene map (mapping) and track the camera motion (localization) jointly, also requiring tighter runtime requirements. Most revised methods focus mainly on either mapping or localization, depending on the main application. Constructing accurate world representations in an SfM/VSLAM pipeline often recalls non-linear optimization schemes that are unfeasible for dense estimates, being also more demanding computationally.

Acknowledgments

We acknowledge the financial support from the Fundação de Amparo à Pesquisa do Estado do Rio Grande do Sul (FAPERGS - Brazil), the Conselho Nacional de Desenvolvimento Científico e Tecnológico (CNPq - Brazil), and the Coordenação de Aperfeiçoamento de Pessoal de Nível Superior (CAPES - Brazil).

References

- [1] F.-E. Wang, H.-N. Hu, H.-T. Cheng, J.-T. Lin, S.-T. Yang, M.-L. Shih, H.-K. Chu, and M. Sun. Self-supervised Learning of Depth and Camera Motion from 360° Videos. volume 11364, pages 53–68. Asian Conference on Computer Vision, 2018.
- [2] M. Schönbein and A. Geiger. Omnidirectional 3D reconstruction in augmented Manhattan worlds. In *IEEE International Conference on Intelligent Robots and Systems*, 2014.
- [3] J. Moreau, S. Ambellouis, and Y. Ruichek. 3D Reconstruction of Urban Environments Based on Fisheye Stereovision. In *IEEE International Conference on Signal Image Technology and Internet Based Systems*, pages 36–41, 2012.
- [4] C. Fernandez-Labrador, J. M. Facil, A. Perez-Yus, C. Demonceaux, J. Civera, and J. Guerrero. Corners for layout: End-to-end layout recovery from 360 images. *IEEE Robotics and Automation Letters*, pages 1–1, 2020.
- [5] G. Fangi, R. Pierdicca, M. Sturari, and E. S. Malinverni. Improving spherical photogrammetry using 360° OMNI-Cameras: Use cases and new applications. *International Archives of the Photogrammetry, Remote Sensing and Spatial Information Sciences*, 42(2):331–337, 2018.
- [6] H. Kim and A. Hilton. Block world reconstruction from spherical stereo image pairs. *Computer Vision and Image Understanding*, 139:104–121, 2015.
- [7] S. Pathak, A. Moro, A. Yamashita, and H. Asama. Dense 3D reconstruction from two spherical images via optical flow-based equirectangular epipolar rectification. In *IEEE International Conference on Imaging Systems and Techniques*, pages 140–145, 2016.
- [8] S. Pathak, A. Moro, A. Yamashita, and H. Asama. Optical Flow-Based Epipolar Estimation of Spherical Image Pairs for 3D Reconstruction. *SICE Journal of Control, Measurement, and System Integration*, 10(5):476–485, 2017.
- [9] A. Pagani, C. Gava, Y. Cui, B. Krolla, J.-M. Hengen, and D. Stricker. Dense 3d point cloud generation from multiple high-resolution spherical images. In *International Conference on Virtual Reality, Archaeology and Cultural Heritage*, pages 17–24, 2011.
- [10] C. C. Gava and D. Stricker. SPHERA: A unifying structure from motion framework for central projection cameras. *International Conference on Computer Vision Theory and Applications*, 3:285–293, 2015.

- [11] G. Pintore, F. Ganovelli, E. Gobbetti, and R. Scopigno. Mobile mapping and visualization of indoor structures to simplify scene understanding and location awareness. In *European Conference on Computer Vision*, pages 130–145, 2016.
- [12] H. Kim and A. Hilton. Planar urban scene reconstruction from spherical images using facade alignment. *IEEE Image, Video, and Multidimensional Signal Processing Workshop*, pages 1–4, 2013.
- [13] A. Kuhn, T. Price, J.-M. Frahm, and H. Mayer. Down to Earth: Using Semantics for Robust Hypothesis Selection for the Five-Point Algorithm. In *German Conference on Pattern Recognition*, volume 10496, pages 389–400, 2017.
- [14] R. G. de A. Azevedo, N. Birkbeck, F. De Simone, I. Janatra, B. Adsumilli, and P. Frossard. Visual Distortions in 360-degree Videos. *IEEE Transactions on Circuits and Systems for Video Technology*, 30(8):2524–2537, 2020.
- [15] J. Thatte, T. Lian, B. Wandell, and B. Girod. Stacked Omnistereo for virtual reality with six degrees of freedom. In *IEEE Visual Communications and Image Processing*, pages 1–4, 2017.
- [16] H. Kim and A. Hilton. 3D Scene Reconstruction from Multiple Spherical Stereo Pairs. *International Journal of Computer Vision*, 104(1):94–116, 2013.
- [17] N. Silberman and R. Fergus. Indoor scene segmentation using a structured light sensor. In *IEEE International Conference on Computer Vision Workshops*, pages 601–608, 2011.
- [18] R. Lukierski, S. Leutenegger, and A. J. Davison. Rapid free-space mapping from a single omnidirectional camera. In *IEEE European Conference on Mobile Robots*, pages 1–8, 2015.
- [19] H. Kim and A. Hilton. Environment modelling using spherical stereo imaging. In *International Conference on Computer Vision Workshops*, pages 1534–1541, 2009.
- [20] S. M. Seitz, B. Curless, J. Diebel, D. Scharstein, and R. Szeliski. A Comparison and Evaluation of Multi-View Stereo Reconstruction Algorithms. In *IEEE Conference on Computer Vision and Pattern Recognition*, volume 1, pages 519–528, 2006.
- [21] O. Özyeşil, V. Voroninski, R. Basri, and A. Singer. A survey of structure from motion. *Acta Numerica*, pages 305–364, 2017.
- [22] R. A. Hamzah and H. Ibrahim. Literature survey on stereo vision disparity map algorithms. *Journal of Sensors*, 2016:1–23, 2016.
- [23] D. Kumari and K. Kaur. A survey on stereo matching techniques for 3d vision in image processing. *International Journal of Engineering and Manufacturing*, 6(4):40–49, 2016.
- [24] D. Scharstein, R. Szeliski, and R. Zabih. A taxonomy and evaluation of dense two-frame stereo correspondence algorithms. *IEEE Workshop on Stereo and Multi-Baseline Vision*, 47(1):131–140, 2001.
- [25] S. Agarwal, Y. Furukawa, N. Snavely, I. Simon, B. Curless, S. M Seitz, and R. Szeliski. Building rome in a day. *Communications of the ACM*, 54(10):105–112, 2011.
- [26] M. Pollefeys, D. Nistér, J.-M. Frahm, A. Akbarzadeh, P. Mordohai, B. Clipp, C. Engels, D. Gallup, S.-J. Kim, P. Merrell, et al. Detailed real-time urban 3d reconstruction from video. *International Journal of Computer Vision*, 78(2-3):143–167, 2008.
- [27] S. Im, H. Ha, F. Rameau, H.-G. Jeon, G. Choe, and I. S. Kweon. All-around depth from small motion with a spherical panoramic camera. In *European Conference on Computer Vision*, pages 156–172, 2016.
- [28] J. Huang, Z. Chen, D. Ceylan, and H. Jin. 6-DoF VR videos with a single 360-camera. In *IEEE Virtual Reality*, pages 37–44, 2017.
- [29] Adriano Q. de Oliveira, Thiago L. T. da Silveira, Marcelo Walter, and Claudio R. Jung. On the Performance of DIBR Methods When Using Depth Maps from State-of-the-art Stereo Matching Algorithms. In *ICASSP 2019 - 2019 IEEE International Conference on Acoustics, Speech and Signal Processing (ICASSP)*, number Vi, pages 2272–2276. IEEE, 2019.
- [30] K. Tateno, N. Navab, and F. Tombari. Distortion-Aware Convolutional Filters for Dense Prediction in Panoramic Images. *European Conference on Computer Vision*, pages 732–750, 2018.
- [31] D. D. Rees. Panoramic television viewing system, 1970. US Patent No. 3,505,465.
- [32] C. Won, J. Ryu, and J. Lim. SweepNet: Wide-baseline Omnidirectional Depth Estimation. In *International Conference on Robotics and Automation*, pages 6073–6079, 2019.
- [33] K. Wegner, O. Stankiewicz, T. Grajek, and M. Domanski. Depth Estimation from Stereoscopic 360-Degree Video. *IEEE International Conference on Image Processing*, pages 2945–2948, 2018.

- [34] T. L. T. da Silveira and C. R. Jung. Perturbation Analysis of the 8-Point Algorithm: A Case Study for Wide FoV Cameras. In *IEEE Conference on Computer Vision and Pattern Recognition*, pages 11757–11766, 2019.
- [35] M. Eder, P. Moulon, and L. Guan. Pano Poppers: Indoor 3D Reconstruction with a Plane-Aware Network. In *2019 International Conference on 3D Vision (3DV)*, pages 76–84. IEEE, 2019.
- [36] A. Pagani and D. Stricker. Structure from Motion using full spherical panoramic cameras. In *IEEE International Conference on Computer Vision Workshops*, pages 375–382, 2011.
- [37] N. Zioulis, A. Karakottas, D. Zarpalas, F. Alvarez, and P. Daras. Spherical View Synthesis for Self-Supervised 360° Depth Estimation. *Conference on 3D Vision*, pages 690–699, 2019.
- [38] B. Luo, F. Xu, C. Richardt, and J.-H. Yong. Parallax360: Stereoscopic 360° Scene Representation for Head-Motion Parallax. *IEEE Transactions on Visualization and Computer Graphics*, 24(4):1545–1553, 2018.
- [39] A. Serrano, I. Kim, Z. Chen, S. DiVerdi, D. Gutierrez, A. Hertzmann, and B. Masia. Motion parallax for 360° RGBD video. *IEEE Transactions on Visualization and Computer Graphics*, 25(5):1817–1827, 2019.
- [40] J. Jeong, D. Jang, J. Son, and E.-S. Ryu. 3DoF+ 360 Video Location-Based Asymmetric Down-Sampling for View Synthesis to Immersive VR Video Streaming. *Sensors*, 18(9), 2018.
- [41] T. L. T. da Silveira and C. R. Jung. Dense 3D Scene Reconstruction from Multiple Spherical Images for 3-DoF+ VR Applications. In *IEEE Conference on Virtual Reality and 3D User Interfaces*, pages 9–18, 2019.
- [42] M. Wien, J. M. Boyce, T. Stockhammer, and W. Peng. Standardization status of immersive video coding. *IEEE Journal on Emerging and Selected Topics in Circuits and Systems*, 9(1):5–17, 2019.
- [43] M. Eder, M. Shvets, J. Lim, and J.-M. Frahm. Tangent images for mitigating spherical distortion. In *IEEE Conference on Computer Vision and Pattern Recognition*, 2020.
- [44] J. Cruz-Mota, I. Bogdanova, B. Paquier, M. Bierlaire, and J. P. Thiran. Scale invariant feature transform on the sphere: Theory and applications. *International Journal of Computer Vision*, 98(2):217–241, 2012.
- [45] Y.-C. Su and K. Grauman. Learning Spherical Convolution for Fast Features from 360° Imagery. In *Conference on Neural Information Processing Systems*, pages 529–539. 2017.
- [46] D. Gledhill, G. Yun Tian, D. Taylor, and D. Clarke. Panoramic imaging - A review. *Computers and Graphics (Pergamon)*, 27(3):435–445, 2003.
- [47] L. Payá, A. Gil, and O. Reinoso. A state-of-the-art review on mapping and localization of mobile robots using omnidirectional vision sensors. *Journal of Sensors*, 2017:1–20, 2017.
- [48] G. Pintore, C. Mura, F. Ganovelli, L. Fuentes-Perez, R. Pajarola, and E. Gobbetti. State-of-the-art in automatic 3d reconstruction of structured indoor environments. *Computer Graphics Forum*, 39(2), 2020.
- [49] C. Zou, J.-W. Su, C.-H. Peng, A. Colburn, Q. Shan, P. Wonka, H.-K. Chu, and D. Hoiem. Manhattan room layout reconstruction from a single 360° image: A comparative study of state-of-the-art methods. *International Journal of Computer Vision*, pages 1–22, 2021.
- [50] Z. Kang, J. Yang, Z. Yang, and S. Cheng. A review of techniques for 3d reconstruction of indoor environments. *ISPRS International Journal of Geo-Information*, 9(5):330, 2020.
- [51] F. Khan, S. Salahuddin, and H. Javidnia. Deep learning-based monocular depth estimation methods - a state-of-the-art review. *Sensors*, 20(8):2272, 2020.
- [52] A. Bhoi. Monocular depth estimation: A survey. *CoRR*, 2019.
- [53] O. Johannsen, K. Honauer, B. Goldluecke, A. Alperovich, F. Battisti, Y. Bok, M. Brizzi, M. Carli, G. Choe, M. Diebold, M. Gutsche, H. Jeon, I. S. Kweon, J. Park, J. Park, H. Schilling, H. Sheng, L. Si, M. Strecke, A. Sulc, Y. Tai, Q. Wang, T. Wang, S. Wanner, Z. Xiong, J. Yu, S. Zhang, and H. Zhu. A taxonomy and evaluation of dense light field depth estimation algorithms. In *IEEE Conference on Computer Vision and Pattern Recognition Workshops*, pages 1795–1812, 2017.
- [54] Yasutaka Furukawa and Carlos Hernández. Multi-view stereo: A tutorial. *Foundations and Trends® in Computer Graphics and Vision*, 9(1-2):1–148, 2015.
- [55] J. Fuentes-Pacheco, J. Ruiz-Ascencio, and J. M. Rendón-Mancha. Visual simultaneous localization and mapping: a survey. *Artificial Intelligence Review*, 43(1):55–81, 2012.
- [56] M. R. U. Saputra, A. Markham, and N. Trigoni. Visual SLAM and structure from motion in dynamic environments. *ACM Computing Surveys*, 51(2):1–36, 2018.
- [57] S. Li and K. Fukumori. Spherical stereo for the construction of immersive vr environment. In *IEEE Virtual Reality*, pages 217–222, 2005.

- [58] S. Li. Binocular spherical stereo. *IEEE Transactions on Intelligent Transportation Systems*, 9(4):589–600, 2008.
- [59] J. Fujiki, A. Torii, and S. Akaho. Epipolar Geometry Via Rectification of Spherical Images. In *Computer Vision/Computer Graphics Collaboration Techniques*, volume 4418, pages 461–471. Springer Berlin Heidelberg, 2007.
- [60] H. Guan and W. A. P. Smith. Structure-From-Motion in Spherical Video Using the von Mises-Fisher Distribution. *IEEE Transactions on Image Processing*, 26(2):711–723, 2017.
- [61] B. Krolla, M. Diebold, B. Goldlücke, and D. Stricker. Spherical light fields. *British Machine Vision Conference*, (67.1-67.12), 2014.
- [62] T. Akihiko, I. Atsushi, and N. Ohnishi. Two-and three-view geometry for spherical cameras. *Workshop on Omnidirectional Vision, Camera Networks and Non-classical Cameras*, 105:29–34, 2005.
- [63] R. Hartley and A. Zisserman. *Multiple View Geometry in Computer Vision*. Cambridge, 2003.
- [64] S. Pathak, A. Moro, H. Fujii, A. Yamashita, and H. Asama. 3D reconstruction of structures using spherical cameras with small motion. In *International Conference on Control, Automation and Systems*, pages 117–122, 2016.
- [65] J. Yang, H. Li, and Y. Jia. Optimal Essential Matrix Estimation via Inlier-Set Maximization. In *European Conference on Computer Vision*, number PART 1, pages 111–126. 2014.
- [66] R. Hartley. In defense of the eight-point algorithm. *IEEE Transactions on Pattern Analysis and Machine Intelligence*, 19(6):580–593, 1997.
- [67] D. Nistér. An efficient solution to the five-point relative pose problem. *IEEE Transactions on Pattern Analysis and Machine Intelligence*, 26(6):756–770, 2004.
- [68] H. C. Longuet-Higgins. A computer algorithm for reconstructing a scene from two projections. In *Readings in Computer Vision*, pages 61 – 62. Morgan Kaufmann, 1987.
- [69] Y. I. Abdel-Aziz and H. M Karara. Direct linear transformation from comparator coordinates into object space in close-range photogrammetry. In *Proceedings of the ASP Symposium on Close-Range Photogrammetry*, pages 1–18, 1971.
- [70] T. Brodsky, C. Fermüller, and Y. Aloimonos. Directions of motion fields are hardly ever ambiguous. *International Journal of Computer Vision*, 26(1):5–24, 1998.
- [71] J. D. Adarve and R. Mahony. Spherpix: A data structure for spherical image processing. *IEEE Robotics and Automation Letters*, 2(2):483–490, 2017.
- [72] S. K. Nayar. Catadioptric Omnidirectional Camera*. In *Conference on Computer Vision and Pattern Recognition*, pages 482–488, 1997.
- [73] F. Huang, R. Klette, and K. Scheibe. *Panoramic Imaging: Sensor-Line Cameras and Laser Range-Finders*. Wiley, 2008.
- [74] I. Labutov, C. Jaramillo, and J. Xiao. Fusing optical flow and stereo in a spherical depth panorama using a single-camera folded catadioptric rig. In *IEEE International Conference on Robotics and Automation*, pages 3092–3097, 2011.
- [75] R. Aggarwal, A. Vohra, and A. M. Namboodiri. Panoramic Stereo Videos with a Single Camera. In *IEEE Conference on Computer Vision and Pattern Recognition*, pages 3755–3763, 2016.
- [76] R. Anderson, D. Gallup, J. T Barron, Janne K., N. Snavely, C. Hernández, S. Agarwal, and S. M. Seitz. Jump: Virtual Reality Video. *ACM Trans. Graph. Article*, 3516(1312):978–1, 2016.
- [77] Y. Shan and S. Li. Descriptor Matching for a Discrete Spherical Image With a Convolutional Neural Network. *IEEE Access*, 6:20748–20755, 2018.
- [78] X. Deng, F. Wu, Y. Wu, and C. Wan. Automatic spherical panorama generation with two fisheye images. In *World Congress on Intelligent Control and Automation*, 2008.
- [79] I. Lo, K. Shih, and H. H. Chen. Image stitching for dual fisheye cameras. In *IEEE International Conference on Image Processing*, pages 3164–3168, 2018.
- [80] R. Jung, A. Ss J. Lee, A. Ashtari, and J.-C. Bazin. Deep360Up: A Deep Learning-Based Approach for Automatic VR Image Upright Adjustment. In *IEEE Conference on Virtual Reality and 3D User Interfaces*, pages 1–8, 2019.
- [81] B. Coors, A. P. Condurache, and A. Geiger. SphereNet: Learning spherical representations for detection and classification in omnidirectional images. *European Conference on Computer Vision*, pages 525–541, 2018.

- [82] Q. Zhao, W. Feng, L. Wan, and J. Zhang. SPHORB: A Fast and Robust Binary Feature on the Sphere. *International Journal of Computer Vision*, 113(2):143–159, 2014.
- [83] C. C. Gava, D. Stricker, and S. Yokota. Dense Scene Reconstruction from Spherical Light Fields. In *IEEE International Conference on Image Processing*, pages 4178–4182, 2018.
- [84] J. Xiao, Krista A. E., A. Oliva, and A. Torralba. Recognizing scene viewpoint using panoramic place representation. In *IEEE Conference on Computer Vision and Pattern Recognition*, pages 2695–2702, 2012.
- [85] L. S. Ferreira, L. Sacht, and L. Velho. Local Moebius transformations applied to omnidirectional images. *Computers & Graphics*, 68:77–83, 2017.
- [86] Y. Sun, A. Lu, and L. Yu. Weighted-to-Spherically-Uniform Quality Evaluation for Omnidirectional Video. *IEEE Signal Processing Letters*, 24(9):1–1, 2017.
- [87] T. L. T. da Silveira, L. P. Dalaqua, and C. R. Jung. Indoor Depth Estimation from Single Spherical Images. In *IEEE International Conference on Image Processing*, pages 2935–2939, 2018.
- [88] Z. Zhang, H. Rebecq, C. Forster, and D. Scaramuzza. Benefit of large field-of-view cameras for visual odometry. *IEEE International Conference on Robotics and Automation*, pages 801–808, 2016.
- [89] F. Dai, C. Zhu, Y. Ma, J. Cao, Q. Zhao, and Y. Zhang. Freely Explore the Scene with 360° Field of View. In *IEEE Conference on Virtual Reality and 3D User Interfaces*, pages 888–889, 2019.
- [90] S. Song, A. Zeng, A. X. Chang, M. Savva, S. Savarese, and T. Funkhouser. Im2Pano3D: Extrapolating 360° Structure and Semantics Beyond the Field of View. In *IEEE/CVF Conference on Computer Vision and Pattern Recognition*, volume 1, pages 3847–3856, 2018.
- [91] H. Guan and W. A. P. Smith. BRISKS: Binary Features for Spherical Images on a Geodesic Grid. In *IEEE Conference on Computer Vision and Pattern Recognition*, pages 4886–4894, 2017.
- [92] M. Eder and J.-M. Frahm. Convolutions on Spherical Images. *IEEE Conference on Computer Vision and Pattern Recognition Workshops*, 2019.
- [93] Y. Lee, J. Jeong, J. Yun, W. Cho, and K.-J. Yoon. Spherephd: Applying cnns on 360° images with non-euclidean spherical polyhedron representation. *IEEE Transactions on Pattern Analysis and Machine Intelligence*, pages 1–1, 2020.
- [94] M. Defferrard, M. Milani, F. Gusset, and N. Perraudin. DeepSphere: a graph-based spherical cnn. In *International Conference on Learning Representations*, 2020.
- [95] S.-T. Yang, F.-E. Wang, C.-H. Peng, P. Wonka, M. Sun, and H.-K. Chu. Dula-net: A dual-projection network for estimating room layouts from a single RGB panorama. In *IEEE Conference on Computer Vision and Pattern Recognition*, pages 3363–3372, 2019.
- [96] A. Saxena, S. H. Chung, and A. Y. Ng. Learning depth from single monocular images. In *Advances in Neural Information Processing Systems*, pages 1161–1168, 2006.
- [97] D. Eigen, C. Puhrsch, and R. Fergus. Depth map prediction from a single image using a multi-scale deep network. In *International Conference on Neural Information Processing Systems*, pages 2366–2374, 2014.
- [98] J. Košecká and W. Zhang. Video compass. In *European Conference on Computer Vision*, pages 476–490, 2002.
- [99] A. Mallya and S. Lazebnik. Learning informative edge maps for indoor scene layout prediction. In *IEEE International Conference on Computer Vision*, pages 936–944, 2015.
- [100] G. P. de La Garanderie, A. A. Abarghouei, and T. P. Breckon. Eliminating the blind spot: Adapting 3D object detection and monocular depth estimation to 360° Panoramic Imagery. *European Conference on Computer Vision*, pages 812–830, 2018.
- [101] H.-Y. Shum, M. Han, and R. Szeliski. Interactive construction of 3d models from panoramic mosaics. In *IEEE Conference on Computer Vision and Pattern Recognition*, pages 427–433, 1998.
- [102] H. Yang and H. Zhang. Modeling room structure from indoor panorama. In *ACM SIGGRAPH International Conference on Virtual-Reality Continuum and Its Applications in Industry*, pages 47–55, 2014.
- [103] H. Jia and S. Li. Estimating structure of indoor scene from a single full-view image. In *IEEE International Conference on Robotics and Automation*, pages 4851–4858, 2015.
- [104] K. Fukano, Y. Mochizuki, S. Iizuka, E. Simo-Serra, A. Sugimoto, and H. Ishikawa. Room reconstruction from a single spherical image by higher-order energy minimization. In *International Conference on Pattern Recognition*, pages 1768–1773, 2016.

- [105] G. Pintore, V. Garro, F. Ganovelli, E. Gobbetti, and M. Agus. Omnidirectional image capture on mobile devices for fast automatic generation of 2.5d indoor maps. In *IEEE Winter Conference on Applications of Computer Vision*, pages 1–9, 2016.
- [106] J. Xu, B. Stenger, T. Kerola, and T. Tung. Pano2cad: Room layout from a single panorama image. In *IEEE Winter Conference on Applications of Computer Vision*, pages 354–362, 2017.
- [107] C. Fernandez-Labrador, A. Perez-Yus, G. Lopez-Nicolas, and J. J. Guerrero. Layouts from panoramic images with geometry and deep learning. *IEEE Robotics and Automation Letters*, 3(4):3153–3160, 2018.
- [108] C. Fernandez-Labrador, J. M. Facil, A. Perez-Yus, c. Demonceaux, and J. J. Guerrero. PanoRoom: From the Sphere to the 3D Layout. pages 1–6, 2018.
- [109] C. Zou, A. Colburn, Q. Shan, and D. Hoiem. LayoutNet: Reconstructing the 3D Room Layout from a Single RGB Image. In *IEEE/CVF Conference on Computer Vision and Pattern Recognition*, pages 2051–2059, 2018.
- [110] C. Sun, C.-W. Hsiao, M. Sun, and H.-T. Chen. HorizonNet: Learning Room Layout with 1D Representation and Pano Stretch Data Augmentation. pages 1047–1056, 2019.
- [111] G. Pintore, M. Agus, and E. Gobbetti. AtlantaNet: Inferring the 3D indoor layout from a single 360 image beyond the Manhattan world assumption. In *European Conference on Computer Vision*, 2020.
- [112] Nikolaos Zioulis, Federico Alvarez, Dimitrios Zarpalas, and Petros Daras. Single-shot cuboids: Geodesics-based end-to-end manhattan aligned layout estimation from spherical panoramas, 2021.
- [113] H. Yang and H. Zhang. Efficient 3D Room Shape Recovery from a Single Panorama. In *IEEE Conference on Computer Vision and Pattern Recognition*, volume 2016-Decem, pages 5422–5430, 2016.
- [114] Y. Yang, R. Liu, and S. B. Kang. Automatic 3D Indoor Scene Modeling from Single Panorama. In *Proceedings of the IEEE Computer Society Conference on Computer Vision and Pattern Recognition*, page 5430. IEEE, 2018.
- [115] Cheng Sun, Min Sun, and Hwann-Tzong Chen. Hohonet: 360 indoor holistic understanding with latent horizontal features. pages 2573–2582, 2021.
- [116] L. Jin, Y. Xu, J. Zheng, J. Zhang, R. Tang, S. Xu, J. Yu, and S. Gao. Geometric structure based and regularized depth estimation from 360 indoor imagery. In *IEEE Conference on Computer Vision and Pattern Recognition*, pages 889–898, 2020.
- [117] Fu-En Wang, Yu-Hsuan Yeh, Min Sun, Wei-Chen Chiu, and Yi-Hsuan Tsai. Led2-net: Monocular 360deg layout estimation via differentiable depth rendering. pages 12956–12965, 2021.
- [118] N. Zioulis, A. Karakottas, D. Zarpalas, and P. Daras. OmniDepth: Dense Depth Estimation for Indoors Spherical Panoramas. In *European Conference on Computer Vision*, pages 453–471. 2018.
- [119] Fu-En Wang, Yu-Hsuan Yeh, Min Sun, Wei-Chen Chiu, and Yi-Hsuan Tsai. Bifuse: Monocular 360 depth estimation via bi-projection fusion. In *Proceedings of the IEEE/CVF Conference on Computer Vision and Pattern Recognition (CVPR)*, 2020.
- [120] Hualie Jiang, Zhe Sheng, Siyu Zhu, Zilong Dong, and Rui Huang. Unifuse: Unidirectional fusion for 360° panorama depth estimation. *IEEE Robotics and Automation Letters*, 6(2):1519–1526, 2021.
- [121] J. Redmon, S. Divvala, R. Girshick, and A. Farhadi. You only look once: Unified, real-time object detection. In *IEEE Conference on Computer Vision and Pattern Recognition (CVPR)*, pages 779–788, 2016.
- [122] O. Ronneberger, P. Fischer, and T. Brox. U-net: Convolutional networks for biomedical image segmentation. In *Medical Image Computing and Computer-Assisted Intervention*, pages 234–241, 2015.
- [123] P. K. Lai, S. Xie, J. Lang, and R. Laquarere. Real-Time Panoramic Depth Maps from Omni-directional Stereo Images for 6 DoF Videos in Virtual Reality. *IEEE Conference on Virtual Reality and 3D User Interfaces*, pages 405–412, 2019.
- [124] Tsun-Hsuan Wang, Hung-Jui Huang, Juan-Ting Lin, Chan-Wei Hu, Kuo-Hao Zeng, and Min Sun. Omnidirectional CNN for visual place recognition and navigation. In *2018 IEEE International Conference on Robotics and Automation (ICRA)*, pages 2341–2348. IEEE, 2018.
- [125] Stefan Schubert, Peer Neubert, Johannes Pöschmann, and Peter Protzel. Circular convolutional neural networks for panoramic images and laser data. In *2019 IEEE Intelligent Vehicles Symposium (IV)*, pages 653–660. IEEE, 2019.
- [126] T. S. Cohen, M. Geiger, J. Köhler, and M. Welling. Spherical cnns. *International Conference on Learning Representations*, 2018.
- [127] C. Esteves, C. Allen-Blanchette, A. Makadia, and K. Daniilidis. Learning so(3) equivariant representations with spherical cnns. In *European Conference on Computer Vision*, 2018.

- [128] C. "M." Jiang, J. Huang, K. Kashinath, Prabhat, P. Marcus, and M. Niessner. Spherical cnns on unstructured grids. In *International Conference on Learning Representations*, 2019.
- [129] Y. Lee, J. Jeong, J. Yun, W. Cho, and K.-J. Yoon. Spherephd: Applying cnns on a spherical polyhedron representation of 360 images. In *IEEE Conference on Computer Vision and Pattern Recognition*, pages 9181–9189, 2019.
- [130] F. Zhao, S. Xia, Z. Wu, D. Duan, L. Wang, W. Lin, J. Gilmore, and G. Li. Spherical u-net on cortical surfaces: Methods and applications. In *International Conference on Information Processing in Medical Imaging*, 2019.
- [131] R. Liu, J. Lehman, P. Molino, F. P. Such, E. Frank, A. Sergeev, and J. Yosinski. An intriguing failing of convolutional neural networks and the CoordConv solution. In *Advances in Neural Information Processing Systems*, pages 9605–9616, 2018.
- [132] S. Xie, P. K. Lai, R. Laganiere, and J. Lang. Effective convolutional neural network layers in flow estimation for omni-directional images. In *Conference on 3D Vision*, pages 671–680, 2019.
- [133] J. Dai, H. Qi, Y. Xiong, Y. Li, G. Zhang, H. Hu, and Y. Wei. Deformable convolutional networks. In *IEEE International Conference on Computer Vision*, pages 764–773, 2017.
- [134] Z. Zhang, Y. Xu, J. Yu, and S. Gao. Saliency detection in 360° videos. In *European Conference on Computer Vision*, pages 504 – 520, 2018.
- [135] P. Frossard and R. Khasanova. Graph-based classification of omnidirectional images. In *IEEE International Conference on Computer Vision Workshops*, pages 860–869, 2017.
- [136] H. Yang and H. Zhang. Indoor structure understanding from single 360 cylindrical panoramic image. In *International Conference on Computer-Aided Design and Computer Graphics*, pages 421–422, 2013.
- [137] Y. Zhang, S. Song, P. Tan, and J. Xiao. PanoContext: A whole-room 3D context model for panoramic scene understanding. In *European Conference on Computer Vision*, 2014.
- [138] P. F. Felzenszwalb and D. P. Huttenlocher. Efficient graph-based image segmentation. *International Journal of Computer Vision*, 59(2):167–181, 2004.
- [139] R. Cabral and Y. Furukawa. Piecewise planar and compact floorplan reconstruction from images. In *IEEE Conference on Computer Vision and Pattern Recognition*, pages 628–635, 2014.
- [140] Matheus A. Bergmann, Paulo G. L. Pinto, Thiago L. T. da Silveira, and Claudio R. Jung. Gravity alignment for single panorama depth inference. In *Conference on Graphics, Patterns and Images (SIBGRAPI)*, pages 1–8. IEEE, 2021.
- [141] D. Eigen and R. Fergus. Predicting Depth, Surface Normals and Semantic Labels with a Common Multi-scale Convolutional Architecture. In *IEEE International Conference on Computer Vision*, pages 2650–2658, 2015.
- [142] A. Vaswani, N. Shazeer, N. Parmar, J. Uszkoreit, L. Jones, A. N. Gomez, L. Kaiser, and I. Polosukhin. Attention is all you need. *Advances in Neural Information Processing Systems*, 30:5998–6008, 2017.
- [143] R. Zhang. Making convolutional networks shift-invariant again. In *International Conference on Machine Learning*, pages 7324–7334, 2019.
- [144] C. Godard, O. Mac Aodha, and G. J. Brostow. Unsupervised Monocular Depth Estimation with Left-Right Consistency. In *Conference on Computer Vision and Pattern Recognition*, pages 270–279, 2017.
- [145] I. Armeni, S. Sax, A. R. Zamir, and S. Savarese. Joint 2D-3D-Semantic Data for Indoor Scene Understanding. 2017.
- [146] C. Harris and M. Stephens. A Combined Corner and Edge Detector. *Alvey Vision Conference*, pages 23.1–23.6, 1988.
- [147] D. G. Lowe. Distinctive image features from scale-invariant keypoints. *International Journal of Computer Vision*, 60(2):91–110, 2004.
- [148] J.-M. Morel and G. Yu. ASIFT: A New Framework for Fully Affine Invariant Image Comparison. *SIAM Journal on Imaging Sciences*, 2(2):438–469, 2009.
- [149] H. Bay, T. Tuytelaars, and L. Van Gool. Surf: Speeded up robust features. In *European Conference on Computer Vision*, pages 404–417, 2006.
- [150] E. Rosten and T. Drummond. Machine learning for high-speed corner detection. In *European Conference on Computer Vision*, pages 430–443, 2006.
- [151] M. Calonder, V. Lepetit, M. Ozuysal, T. Trzcinski, C. Strecha, and P. Fua. Brief: Computing a local binary descriptor very fast. *IEEE Transactions on Pattern Analysis and Machine Intelligence*, 34(7):1281–1298, 2011.

- [152] S. Leutenegger, M. Chli, and R. Y. Siegwart. Brisk: Binary robust invariant scalable keypoints. In *2011 International Conference on Computer Vision*, pages 2548–2555, 2011.
- [153] E. Rublee, V. Rabaud, K. Konolige, and G. Bradski. Orb: An efficient alternative to sift or surf. In *International Conference on Computer Vision*, page 2564–2571, 2011.
- [154] P. Alcantarilla, A. Bartoli, and A. J. Davison. KAZE Features. In *European Conference on Computer Vision*, pages 214–227. Springer Berlin Heidelberg, 2012.
- [155] P. Alcantarilla, J. Nuevo, and A. Bartoli. Fast Explicit Diffusion for Accelerated Features in Nonlinear Scale Spaces. *British Machine Vision Conference*, pages 13.1–13.11, 2013.
- [156] C. Leng, H. Zhang, B. Li, G. Cai, Z. Pei, and L. He. Local feature descriptor for image matching: A survey. *IEEE Access*, 7:6424–6434, 2019.
- [157] T. L. T. da Silveira and C. R. Jung. Evaluation of Keypoint Extraction and Matching for Pose Estimation Using Pairs of Spherical Images. *Conference on Graphics, Patterns and Images*, pages 374–381, 2017.
- [158] H. Guan, W. A. P. Smith, and P. Ren. Corner detection in spherical images via the accelerated segment test on a geodesic grid. In *International Symposium on Visual Computing*, pages 407–415, 2013.
- [159] R. Kitamura, S. Li, and I. Nakanishi. Spherical fast corner detector. In *IEEE International Conference on Mechatronics and Automation*, pages 2597–2602, 2015.
- [160] D. DeTone, T. Malisiewicz, and A. Rabinovich. Superpoint: Self-supervised interest point detection and description. In *2018 IEEE/CVF Conference on Computer Vision and Pattern Recognition Workshops (CVPRW)*, pages 337–33712, 2018.
- [161] M. Zhai, X. Xiang, N. Lv, and X. Kong. Optical flow and scene flow estimation: A survey. *Pattern Recognition*, 114:107861, 2021.
- [162] B. Xu, S. Pathak, H. Fujii, A. Yamashita, and H. Asama. Optical flow-based video completion in spherical image sequences. In *IEEE International Conference on Robotics and Biomimetics*, pages 388–395, 2016.
- [163] P. Weinzaepfel, J. Revaud, Z. Harchaoui, and C. Schmid. DeepFlow: Large displacement optical flow with deep matching. *IEEE International Conference on Computer Vision*, pages 1385–1392, 2013.
- [164] Y. Mochizuki and A. Imiya. Featureless visual navigation using optical flow of omnidirectional image sequence. In *IEEE International Conference on Simulation, Modeling, and Programming for Autonomous Robots*, pages 307–318, 2008.
- [165] B. K.P. Horn and B. G. Schunck. Determining optical flow. *Artificial Intelligence*, 17(1):185 – 203, 1981.
- [166] G. J. Conklin and S. S. Hemami. Multi-resolution motion estimation. In *IEEE International Conference on Acoustics, Speech, and Signal Processing*, volume 4, pages 2873–2876 vol.4, 1997.
- [167] I. Tomic, I. Bogdanova, P. Frossard, and P. Vanderghyest. Multiresolution motion estimation for omnidirectional images. In *European Signal Processing Conference*, pages 1–4, 2005.
- [168] Y. Mochizuki and A. Imiya. Multiresolution optical flow computation of spherical images. In *Computer Analysis of Images and Patterns*, pages 348–355, 2011.
- [169] A. Radgui, C. Demonceaux, E. M. Mouaddib, M. Rziza, and D. Aboutajdine. Optical flow estimation from multichannel spherical image decomposition. *Computer Vision and Image Understanding*, 115(9):1263–1272, 2011.
- [170] B. Alibouch, A. Radgui, C. Demonceaux, M. Rziza, and D. Aboutajdine. A phase-based framework for optical flow estimation on omnidirectional images. *Signal, Image and Video Processing*, 10:1–8, 2014.
- [171] L. Bagnato, P. Frossard, and P. Vanderghyest. Optical flow and depth from motion for omnidirectional images using a tv-11 variational framework on graphs. In *IEEE International Conference on Image Processing*, pages 1469–1472, 2009.
- [172] C. Zach, T. Pock, and H. Bischof. A duality based approach for realtime tv-11 optical flow. In *Pattern Recognition*, pages 214–223, 2007.
- [173] D. Kim, S. Pathak, A. Moro, R. Komatsu, A. Yamashita, and H. Asama. E-cnn: Accurate spherical camera rotation estimation via uniformization of distorted optical flow fields. In *IEEE International Conference on Acoustics, Speech and Signal Processing*, pages 2232–2236, 2019.
- [174] D. Sun, X. Yang, M. Liu, and J. Kautz. Pwc-net: Cnns for optical flow using pyramid, warping, and cost volume. In *IEEE/CVF Conference on Computer Vision and Pattern Recognition*, pages 8934–8943, 2018.

- [175] A. Dosovitskiy, P. Fischer, E. Ilg, P. Häusser, C. Hazirbas, V. Golkov, P. v. d. Smagt, D. Cremers, and T. Brox. FlowNet: Learning optical flow with convolutional networks. In *IEEE International Conference on Computer Vision*, pages 2758–2766, 2015.
- [176] A. Ranjan and M. J. Black. Optical flow estimation using a spatial pyramid network. In *IEEE/CVF Conference on Computer Vision and Pattern Recognition*, 2016.
- [177] C.-O. Artizzu, H. Zhang, G. Allibert, and C. Démonceaux. OmniFlowNet: a Perspective Neural Network Adaptation for Optical Flow Estimation in Omnidirectional Images. In *International Conference on Pattern Recognition*, 2021.
- [178] Keshav Bhandari, Ziliang Zong, and Yan Yan. Revisiting optical flow estimation in 360 videos. In *IEEE International Conference on Pattern Recognition*, pages 8196–8203, 2021.
- [179] T. Hui, X. Tang, and C. C. Loy. LiteflowNet: A lightweight convolutional neural network for optical flow estimation. In *IEEE Conference on Computer Vision and Pattern Recognition*, pages 8981–8989, 2018.
- [180] Z. Arican and P. Frossard. Dense disparity estimation from omnidirectional images. In *IEEE Conference on Advanced Video and Signal Based Surveillance*, pages 399–404, 2007.
- [181] S. Pathak, A. Moro, H. Fujii, A. Yamashita, and H. Asama. Virtual reality with motion parallax by dense optical flow-based depth generation from two spherical images. In *IEEE/SICE International Symposium on System Integration*, pages 887–892, 2017.
- [182] H. Kim, T. d. Campos, and A. Hilton. Room layout estimation with object and material attributes information using a spherical camera. In *Conference on 3D Vision*, pages 519–527, 2016.
- [183] H. Kim, L. Remaggi, P. J. Jackson, F. M. Fazi, and A. Hilton. 3d room geometry reconstruction using audio-visual sensors. In *Conference on 3D Vision*, pages 621–629, 2017.
- [184] Ning-Hsu Wang, Bolivar Solarte, Yi-Hsuan Tsai, Wei-Chen Chiu, and Min Sun. 360sd-net: 360° stereo depth estimation with learnable cost volume. *IEEE International Conference on Robotics and Automation*, 2020.
- [185] M. Roxas and T. Oishi. Variational fisheye stereo. *IEEE Robotics and Automation Letters*, 5(2):1303–1310, 2020.
- [186] B. D. Lucas and T. Kanade. An iterative image registration technique with an application to stereo vision. In *International Joint Conference on Artificial Intelligence*, pages 674–679, 1981.
- [187] J. R. Shewchuk. Reprint of: Delaunay refinement algorithms for triangular mesh generation. *Computational Geometry: Theory and Applications*, 2014.
- [188] R. J. Radke. *Computer Vision for Visual Effects*. Cambridge, 2012.
- [189] V. Kolmogorov and R. Zabih. Multi-camera scene reconstruction via graph cuts. In *European Conference on Computer Vision*, pages 82–96, 2002.
- [190] K. Wegner, O. Stankiewicz, and M. Domański. Depth based view blending in view synthesis reference software (vsrs), 2015. ISO/IEC JTC1/SC29/WG11 MPEG2015, M37232, Geneva, Switzerland.
- [191] R. S. Overbeck, D. Erickson, D. Evangelakos, M. Pharr, and P. Debevec. A system for acquiring, processing, and rendering panoramic light field stills for virtual reality. *ACM Transactions on Graphics (TOG)*, 37(6):1–15, 2018.
- [192] T. Bertel, N. D. F. Campbell, and C. Richardt. Megaparallax: Casual 360 panoramas with motion parallax. *IEEE Transactions on Visualization and Computer Graphics*, 25(5):1828–1835, 2019.
- [193] T. Bertel, M. Yuan, R. Lindroos, and C. Richardt. Omniphotos: Casual 360° vr photography. *ACM Transactions on Graphics*, 39(6):1–12, 2020.
- [194] H. Kim and A. Hilton. 3d modelling of static environments using multiple spherical stereo. In Kiriakos N. Kutulakos, editor, *European Conference on Computer Vision*, pages 169–183, 2010.
- [195] C. Won, J. Ryu, and J. Lim. OmniMVS: End-to-End Learning for Omnidirectional Stereo Matching. In *IEEE International Conference on Computer Vision*, 2019.
- [196] C. Won, J. Ryu, and J. Lim. End-to-end learning for omnidirectional stereo matching with uncertainty prior. *IEEE Transactions on Pattern Analysis and Machine Intelligence*, 2020.
- [197] A. Torii, M. Havlena, and T. Pajdla. From google street view to 3d city models. In *International Conference on Computer Vision Workshops*, pages 2188–2195, 2009.
- [198] B. Micusik and J. Kosecka. Piecewise planar city 3d modeling from street view panoramic sequences. In *IEEE Conference on Computer Vision and Pattern Recognition*, pages 2906–2912, 2009.

- [199] L. Barazzetti, M. Previtali, and F. Roncoroni. 3d modelling with the samsung gear 360. In *Virtual Reconstruction and Visualization of Complex Architectures*, volume 42, pages 85–90. International Society for Photogrammetry and Remote Sensing, 2017.
- [200] L. Bagnato, P. Frossard, and P. Vanderghelynst. A variational framework for structure from motion in omnidirectional image sequences. *Journal of Mathematical Imaging and Vision*, 41(3):182–193, 2011.
- [201] D. Caruso, J. Engel, and D. Cremers. Large-scale direct SLAM for omnidirectional cameras. *International Conference on Intelligent Robots and Systems*, pages 141–148, 2015.
- [202] G. Pintore, F. Ganovelli, R. Pintus, R. Scopigno, and E. Gobbetti. Recovering 3d indoor floor plans by exploiting low-cost spherical photography. In *Pacific Conference on Computer Graphics and Applications*, PG ’18, pages 45–48, 2018.
- [203] G. Pintore, R. Pintus, F. Ganovelli, R. Scopigno, and E. Gobbetti. Recovering 3d existing-conditions of indoor structures from spherical images. *Computers and Graphics*, 77:16 – 29, 2018.
- [204] Marc Levoy and Pat Hanrahan. Light field rendering. In *Proceedings of the 23rd annual conference on Computer graphics and interactive techniques*, pages 31–42, 1996.
- [205] Robert C Bolles, H Harlyn Baker, and David H Marimont. Epipolar-plane image analysis: An approach to determining structure from motion. *International Journal of Computer Vision*, 1(1):7–55, 1987.
- [206] Marc Levoy. Light fields and computational imaging. *Computer*, 39(8):46–55, 2006.
- [207] Yuichi Taguchi, Amit Agrawal, Ashok Veeraraghavan, Srikumar Ramalingam, and Ramesh Raskar. Axial-cones: Modeling spherical catadioptric cameras for wide-angle light field rendering. *ACM Trans. Graph.*, 29(6):172, 2010.
- [208] Clemens Birklbauer and Oliver Bimber. Panorama light-field imaging. In *Computer Graphics Forum*, volume 33, pages 43–52. Wiley Online Library, 2014.
- [209] M. Bentsen, G. Evensen, H. Drange, and A. D. Jenkins. Coordinate transformation on a sphere using conformal mapping. *Monthly Weather Review*, 127(12):2733–2740, 1999.
- [210] Vincent Sitzmann, Semon Rezchikov, William T Freeman, Joshua B Tenenbaum, and Fredo Durand. Light field networks: Neural scene representations with single-evaluation rendering. 2021.
- [211] Jonathan T Barron, Andrew Adams, YiChang Shih, and Carlos Hernández. Fast bilateral-space stereo for synthetic defocus. In *Proceedings of the IEEE Conference on Computer Vision and Pattern Recognition*, pages 4466–4474, 2015.
- [212] Shinya Sumikura, Mikiya Shibuya, and Ken Sakurada. Openslam: a versatile visual slam framework. In *Proceedings of the 27th ACM International Conference on Multimedia*, pages 2292–2295, 2019.
- [213] P. J. Besl and N. D. McKay. A method for registration of 3-d shapes. volume 14, pages 239–256, 1992.
- [214] S. Shen. Accurate multiple view 3d reconstruction using patch-based stereo for large-scale scenes. *IEEE Transactions on Image Processing*, 22(5):1901–1914, 2013.
- [215] Y. Furukawa and J. Ponce. Accurate, Dense, and Robust Multi-View Stereopsis. In *IEEE Conference on Computer Vision and Pattern Recognition*, volume 32, pages 1–8, 2007.
- [216] A. T. Wood. Simulation of the von mises fisher distribution. *Communications in Statistics - Simulation and Computation*, 23(1):157–164, 1994.
- [217] E. S. L. Gastal and M. M. Oliveira. Domain transform for edge-aware image and video processing. *ACM Trans. Graph.*, 30(4):69:1–69:12, 2011.
- [218] R. Achanta, A. Shaji, K. Smith, A. Lucchi, P. Fua, and S. Süsstrunk. Slic superpixels compared to state-of-the-art superpixel methods. *IEEE Transactions on Pattern Analysis and Machine Intelligence*, 34(11):2274–2282, 2012.
- [219] F. Kangni and R. Laganieri. Orientation and pose recovery from spherical panoramas. In *IEEE International Conference on Computer Vision*, pages 1–8, 2007.
- [220] Q. Zhao, F. Dai, Y. Ma, L. Wan, J. Zhang, and Y. Zhang. Spherical Superpixel Segmentation. *IEEE Transactions on Multimedia*, 20(6):1406–1417, 2018.
- [221] Rémi Giraud, Rodrigo Borba Pinheiro, and Yannick Berthoumieu. Generalized shortest path-based superpixels for accurate segmentation of spherical images. pages 2650–2656, 2021.
- [222] Thiago L.T. da Silveira, Adriano Q. de Oliveira, Marcelo Walter, and Cláudio R. Jung. Fast and accurate superpixel algorithms for 360° images. *Signal Processing*, 189:108277, 2021.

- [223] Changhee Won, Hochang Seok, Zhaopeng Cui, Marc Pollefeys, and Jongwoo Lim. Omnislam: Omnidirectional localization and dense mapping for wide-baseline multi-camera systems. pages 559–566, 2020.
- [224] Jia Zheng, Junfei Zhang, Jing Li, Rui Tang, Shenghua Gao, and Zihan Zhou. Structured3d: A large photo-realistic dataset for structured 3d modeling. pages 519–535, 2020.
- [225] A. Chang, A. Dai, T. Funkhouser, M. Halber, M. Niessner, M. Savva, S. Song, A. Zeng, and Y. Zhang. Matterport3d: Learning from rgb-d data in indoor environments. *International Conference on 3D Vision*, 2017.
- [226] S. Song, F. Yu, A. Zeng, A. X Chang, M. Savva, and T. Funkhouser. Semantic scene completion from a single depth image. *IEEE Conference on Computer Vision and Pattern Recognition*, 2017.
- [227] L. Tchammi and D. Huber. The SUMO challenge, 2019.
- [228] Blender Online Community. *Blender - A 3D Modelling and Rendering Package*. Blender Foundation, 2020.
- [229] M. Menze and A. Geiger. Object scene flow for autonomous vehicles. In *IEEE Conference on Computer Vision and Pattern Recognition*, pages 3061–3070, 2015.